This is the peer-reviewed, final accepted version for American Mineralogist, published by the Mineralogical Society of America.
The published version is subject to change. Cite as Authors (Year) Title. American Mineralogist, in press.
DOI: https://doi.org/10.2138/am-2022-8156. http://www.minsocam.org/

Word Count: 8859 **Revision No. 1**

The crystal structure of mineral magadiite, $Na_2Si_{14}O_{28}(OH)_2*8H_2O$

Bernd Marler[1,*], Yaşar Krysiak[2], Isabel Grosskreuz[1], Hermann Gies[1] and Ute Kolb[3]

[1]Institute of Geology, Mineralogy and Geophysics, University of Bochum, DE-44801 Bochum, Germany. Fax: +49 0234 32 14433; Tel: +49 234 32 23514; E-mail: bernd.marler@rub.de

[2]Institute of Inorganic Chemistry, Leibniz University Hannover, Schneiderberg 39, 30167 Hannover, Germany.

[3]Institute of Inorganic Chemistry and Analytical Chemistry, Johannes Gutenberg University Mainz, DE-55122 Mainz, Germany.

ABSTRACT

Magadiite from Lake Magadi was structurally analyzed based on X-ray powder diffraction data. The idealized chemical composition of magadiite is $Na_{16}[Si_{112}O_{224}(OH)_{16}]*64H_2O$ per unit cell. The XRD powder diffraction pattern was indexed in orthorhombic symmetry with lattice

parameters a_0 = 10.5035(9) Å, b_0 = 10.0262(9) Å and c_0 = 61.9608(46) Å. The crystal structure was solved from a synthetic magadiite sample in a complex process using 3D electron diffraction combined with model building as presented in an additional paper. A Rietveld refinement of this structure model performed on a magadiite mineral sample in space group *F2dd* (No. 43) converged to residual values of R_{Bragg} = 0.031 and R_F = 0.026 confirming the structure model. Physico-chemical characterization using solid-state NMR spectroscopy, SEM, TG-DTA, and DRIFT spectroscopy further confirmed the structure. The structure of magadiite contains two enantiomorphic silicate layers of, so far, unknown topology. The dense layers exhibit no porosity or micro-channels and have a thickness of 11.5 Å (disregarding the v. d. Waals radii of the terminal oxygen atoms) and possess a silicon Q^4 to Q^3 ratio of 2.5. 16 out of 32 terminal silanol groups are protonated, the remaining groups compensate the charge of the hydrated sodium cations. Bands of edge-sharing $[Na(H_2O)_{6/1.5}]$ octahedra are intercalated between the silicate layers extending along (110) and (-110). The water molecules are hydrogen bonded to terminal silanol groups with O···O distances of 2.54 Å–2.91 Å. The structure of magadiite is slightly disordered typical for hydrous layer silicates (HLS) which possess only weak interactions between neighboring layers. In this respect, the result of the structure refinement represents a somewhat idealized structure. Nevertheless, the magadiite mineral possesses a higher degree of structural order than any synthetic magadiite sample. The structure analysis also revealed the presence of strong intra-layer hydrogen bonds between the terminal O atoms (silanol/siloxy groups) confirmed by ^{1}H MAS NMR and DRIFT spectroscopy. The surface zone of the silicate layers as well as the inter-layer region containing the $[Na(H_2O)_{6/1.5}]$ octahedra are closely related to the structure of Na-RUB-18.

Keywords: Sodium silicate, structure determination, characterization, layer silicate, Rietveld

INTRODUCTION

Occurrences and properties of magadiite

Magadiite is a mineral known since 1967 (Eugster 1967) and is named after Lake Magadi, Kenya, the location of the initial mineral discovery. Later, other occurrences of magadiite have emerged: Trinity County, California, USA (McAtee, et al. 1968); Mont Saint-Hilaire, Canada (Horváth and Gault 1990); Lake Chad, Chad (Maglione 1970); Alkali Lake, Oregon, USA (Rooney et al. 1969) and Aris phonolites, Windhoek, Namibia (Hudson Institute of Mineralogy 1993-2020) to name a few.

Magadiite typically precipitates form saline brines of alkaline lakes which contain large amounts of soluble silica. According to Jones et al. "high concentrations of SiO_2 can be attributed to reaction of waters with silicates, and subsequent evaporative concentration accompanied by a rise in pH" (Jones et al. 1967). In addition, carbonates, halides, sodium silicates, zeolites, feldspars, iron oxides, quartz and garnet manifest in these deposits as impurities. This fact is attributed to the reaction between the volcanic rocks and brines, which also cause the formation of halite, gaylussite, calcite, villiaumite, strontianite, fluorite and mirabilite from residual brines (Rammlmair 2000).

The type locality of magadiite is Lake Magadi, Kajiado County, Kenya. Lake Magadi is a saline, alkaline lake which is fed by alkaline hot springs and saturated brines with high

concentrations of sodium carbonate. The lake is the most saline of all the lakes in the Eastern Rift Valley and is surrounded by a closed basin at 603 m above sea level. The lake is periodically dry, except for brine pools near the margins, containing a vast deposit of trona (Eugster 1969).

The idealized chemical composition as given by Hans Eugster in 1967 is $Na_2Si_{14}O_{26}(OH)_6*6H_2O$. Magadiite is a soft (Mohs hardness: 2), white, transparent mineral. The experimental density is 2.17 g cm^{-3}; the crystals are birefringent with a biaxial indicatrix and a mean refractive index of 1.48 (Eugster 1967). It appears as white masses of very small plate-like crystals and is often associated with quartz and kenyaite.

The water content of magadiite is obviously quite variable and seems to depend on the ambient atmosphere and/or the pretreatment of the sample prior to chemical analysis (Scholzen et al. 1991). Moreover, a part of the sodium cations can easily be leached from the structure by a mere washing of the crystals with water (Schwieger and Lagaly 2004). As a consequence, different chemical formulas of magadiite are reported in the literature: $Na_2Si_{14}O_{29}*11H_2O$ (Schwieger and Lagaly 2004), $Na_2H_2[Si_{14}O_{30}]*6H_2O$ (Oumi et al. 2008), $Na_2[Si1_4O_{26}]*8H_2O$ (Anthony et al. 2003).

Magadiite is a layered alkali silicate and belongs to the group of Hydrous Layer Silicates (HLSs) (Marler et al. 2021) like the mineral kanemite $Na_4[Si_8O_{16}(OH)_4]*12H_2O$ (Gies et al. 1998; Garvie et al. 1999; Vortmann et al. 1999) or synthetic Na-RUB-18, $Na_8[H_8Si_{32}O_{72}]*32H_2O$ (Vortmann et al. 1997), also known as octosilicate (Schwieger and Lagaly 2004). HLSs, also often named "2D Zeolites" are structurally interesting materials characterized by silicate layers of various topologies. Layers of interconnected [SiO_4]-units that

contain equal numbers of terminal silanol/siloxy groups on either side of the layer are intercalated by cations of low charge density and water molecules.

Synthesis and use of magadiite

HLSs can be used as parent materials to synthesize mesoporous and microporous framework materials by either **expanding** the structures using appropriate methods or by **condensing the silicate layers** topotactically (Marler and Gies 2012). Sirinakorn et al. (Sirinakorn et al. 2018) and Roth et al. (Roth et al. 2016) published review articles on research papers dealing with modifications of layered silicates such as kanemite, makatite, octosilicate and magadiite by ion exchange with organic and inorganic cations, pillaring, silylation of the OH groups and grafting, or introducing of metal nanoparticles. In addition, HLSs can be used as a starting material for zeolite synthesis by classical **hydrothermal treatment** for the synthesis of, e.g., ZSM-5 and ferrierite (Y. Wang et al. 2015) or mordenite (Shi et al. 2013), or applied as precursors to obtain ordered mesoporous three-dimensional silicate frameworks, e.g., mesoporous silica made from kanemite (Kuroda 1996).

Magadiite-type materials are one of the most extensively investigated layered silicates and have frequently been synthesized in the lab by hydrothermal treatment of aqueous reaction mixtures containing sodium, silica and, sometimes, additional compounds like Al or organic molecules. Typical synthesis procedures can be found in the Handbook of Layered Materials by Schwieger and Lagaly (Schwieger and Lagaly 2004). Modified procedures have, for example, been reported by Superti, Bisio and Pastore who synthesized aluminum-modified magadiite

(Superti et al. 2007), by Feng and Balkus who synthesized magadiite using poly(ethylen glycol) as a template (Feng and Balkus 2003), and Sassi et al. who prepared magadiite in a water/alcohol system (Sassi et al. 2005).

Primarily, magadiite has been synthesized to act as a precursor material for a subsequent transformation into porous silicates. Ogawa et al. have conducted extensive research on the modifications of the inter-layer of layered silicates for the application as host-guest systems and photo-functional intercalation compounds (Ogawa and Kuroda 1997; Ogawa and Maeda 1998; Ogawa et al. 2001a, 2001b). A cation exchange with different metallic, organic and organometallic cations has been suggested for the functionalization of magadiite by Kim et al. (C. S. Kim et al. 1997) while ion exchanged magadiite samples were used for the construction of porous pillared layered silicates (Sprung et al. 1990; S. J. Kim et al. 2012). A modification of magadiite with polyethylenimine has been performed by Vieira and Pastore with the intent of applications in CO_2 capture (Vieira and Pastore 2014). Lagaly et al. reported on the attachment of organic functional groups in the inter-layer space covalently bound through the condensation reactions of the silanol groups with chlorosilanes, alkoxysilanes and alcohols (Lagaly et al. 1975; Lagaly 1986; Scholzen et al.1991). Further functionalization was achieved by grafting of the silanol groups with silane coupling reagents (Ruiz-Hitzky et al. 1985; Ogawa and Kuroda 1997; Ogawa and Maeda 1998; Takahashi and Kuroda 2011). Exfoliation of magadiite nano-layers has been conducted by Wang and Pinnavaia, (Z. Wang and Pinnavaia 1998).

This is the peer-reviewed, final accepted version for American Mineralogist, published by the Mineralogical Society of America.
The published version is subject to change. Cite as Authors (Year) Title. American Mineralogist, in press.
DOI: https://doi.org/10.2138/am-2022-8156. http://www.minsocam.org/

Previous structural studies

Although several natural and many synthetic magadiite samples are available, the structure of magadiite remained hidden until now because of the small crystal size, the complex crystal structure and the restricted crystallinity of the materials. The diffraction pattern is characterized by a first strong reflection around 5.7 °2θ (Cu Kα) corresponding to $d \approx 15.5$ Å and broad reflections of different halfwidths. Because of the relatively poor XRD powder diffraction diagrams of all known magadiite samples, even the unit cell dimensions were not unambiguously determinable. Literature unit cell values are presented by Eugster: $a_0 = b_0 = 12.620$ Å, $c_0 = 15.573$ Å, $\beta = 90$ ° (Eugster 1967); McAtee et al.: $a_0 = 7.22$ Å, $b_0 = 15.70$ Å, $c_0 = 6.91$ Å, $\beta = 95.27$ ° (McAtee et al. 1968); Brindley: $a_0 = b_0 = 7.25$ Å, $c_0 = 15.69$ Å, $\beta = 96.8$ ° (Brindley 1969); as well as Ide et. al.: $a_0 = 15.60(3)$ Å, $b_0 = 3.837(7)$ Å, $c_0 = 7.344(14)$ Å, $\alpha = 93.76$ °, $\beta = 95.42$ ° $\gamma = 95.21$ ° (Ide et al. 2018), respectively.

In the past, several attempts have been made to reveal the crystal structure of magadiite based on unit cell dimensions, chemical composition, NMR, Raman and IR spectra and depending on the comparison with the known structures of seemingly related silicates like Na-RUB-18/octosilicate, kanemite, makatite and dachiardite. Only one structural study, which was published recently, used the whole X-ray powder diffraction pattern of magadiite to establish a structure model using a PDF (pair-distribution function) analysis and real-space methods (Ide et al. 2018).

^{23}Na MAS NMR studies showed that magadiite has only one sodium site in its structure (Almond et al. 1996). Moreover, ^{1}H–^{23}Na heteronuclear shift correlation spectra revealed that

strongly hydrogen bonded protons are in close vicinity to the sodium ions. The authors tentatively proposed a coordination number of six for the sodium ions in magadiite. Investigations based on FT-IR and FT-Raman spectra (Huang et al. 1999) seemed to indicate that magadiite exhibits i) a centrosymmetric structure of point group symmetry *2/m*, ii) has a multilayer structure with five- and six-membered rings with Si–O–Si linkages having partly large bond angles near 180 °, iii) a hydrogen bonding system, however, with some hydroxyl groups not involved.

Brandt, Schwieger and Bergk proposed a structure solution developed by model building which was based on the unit cell as determined by Brindley for air-dry magadiite (a_0 = 7.25 Å, b_0 = 7.25 Å,γ = 90 °), basal spacing of the first XRD peak, (d = 15.6 Å) and NMR data. According to this model, three (pseudo) tetragonal layer-like building units consisting of 4- and 8-rings are interconnected along the c_0-axis to form the silicate layer of magadiite (Schwieger et al. 1985; Brandt et al. 1987; Brandt et al. 1988, 1989).

In 1988, Garcés et al. (Garcés 1988) presented a hypothetical structure model of magadiite based on the structure of zeolite dachiardite: "The similarities between the IR and NMR spectra of the layered alkali metal silicates magadiite and sodium octosilicate and those of the zeolites of the mordenite group [...] suggest that the unknown structures of the layered alkali metal silicates may be related to the mordenite-group structures in the same manner that bikitaite is related to $KHSi_2O_5$ and kanemite. A hypothetical structure for magadiite was derived from the structure of dachiardite [...]". The (water-free) model structure, however, has a Q^4 to Q^3 ratio of only two and a chemical composition of $NaSi_6O_{12}(OH)$ with an unusual Si to Na ratio of six. Almond et al.

(Almond et al. 1996) discussed an additional model structure of magadiite by comparing ^{1}H, ^{23}Na and ^{29}Si NMR data. The structure model is based on the structures of layer silicates $KHSi_2O_5$ and EU-19, instead of kanemite. The authors postulate the presence of hydrated Na ions between layers (only one site) and direct hydrogen bonds between silanol groups of neighboring layers.

A very recent structural study on magadiite applied a PDF analysis based on an initial structure model prepared form the octosilicate structure. The authors suggest a triclinic unit cell with $a_0 = 15.750$ Å, $b_0 = 3.930$ Å, $c_0 = 7.365$ Å, $\alpha = 96.38$ °, $\beta = 95.92$ °, $\gamma = 96.18$ ° and a unit cell composition of $Na_{1.44}Si_{10}O_{22}*3H_2O$. According to the PDF model, the silicate layer is rather thick (13.3 Å) and contains intra-layer micro-channels which are presumed to be occupied by sodium ions (Ide et al. 2018; Doustkhah and Ide 2020).

All these attempts to determine the true structure of magadiite failed because of lack of information. The breakthrough concerning the structure solution was finally achieved by using the Automated Diffraction Tomography (ADT) method combined with model building (see below).

EXPERIMENTAL

Sample

The investigated sample was collected from Lake Magadi/Kenya (alluvial channel, east of the township, south of the road). It is the type locality of magadiite described by Eugster (Eugster

1967). Macroscopically, the sample can be described as a white to slightly gray mass of very small crystals. Lumps of magadiite are soft and can easily be disaggregated into a powder sample.

General Characterization

Scanning electron micrographs were taken using a LEO-1530 Gemini electron microscope to study the morphology of the crystals and the homogeneity of the samples. The samples were gold coated by vacuum vapor deposition prior to analysis. For a qualitative chemical analysis, an OXFORD AZtecEnergy X-ray microanalysis system (attached to the electron microscope) was used.

Quantitative chemical analysis was performed by atomic absorption spectroscopy using a Varian SpectrAA 220.

Thermal properties were investigated by simultaneous DTA/TG measurements using a TA Instruments SDT650 thermal analyzer. The samples were heated in synthetic air from 30 °C–1000 °C with a heating rate of 10 °C min^{-1}.

Diffuse reflectance infrared Fourier transform (DRIFT) spectroscopy was performed using a Nicolet 6700 FT-IR spectrometer. 6 mg of sample were mixed with 250 mg of diamond powder to adjust the intensity of the diffuse reflectance. The spectrum was recorded in dry air between 400 cm^{-1}–4000 cm^{-1} with a resolution of 4 cm^{-1}.

Solid state MAS NMR spectra were recorded at room temperature with a Bruker ASX-400 spectrometer using standard Bruker MAS probes, operated at 400.147 MHz (^{1}H) or 79.497 MHz

(^{29}Si). In order to average the chemical shift anisotropies, samples were spun about the magic angle. For each measurement, tetramethylsilane (TMS) was used as a chemical shift standard. Concerning ^{29}Si MAS NMR spectra, HPDEC measurements (800 scans) were performed with a spinning frequency of 4 kHz, a pulse length of 4 μs and a cycle delay time of 60 s for complete relaxation of the nuclei in order to calculate the Q^4 to Q^3 ratio from the signal intensities. The ^{1}H MAS NMR spectra (128 scans) were measured with a spinning frequency of 12.5 kHz, a pulse length of 2 μs, and a cycle delay time of 10 s.

The structure model of the hypothetical condensed, ordered magadiite generated by formally condensing the silicate layers was optimized in a Distance-Least-Squares (DLS) refinement assuming Si–O distances of 1.610 Å, Si–O–Si angles of 150.0 ° and regular O–Si–O angles of the [SiO_4] tetrahedra. For the refinement, the program DLS-76 was used (Baerlocher et al. 1978). A space group symmetry of *F2dd* was assumed for condensed magadiite. Since no experimental parameters were available, lattice parameters were refined in addition.

Structure Analysis

Due to the small size and the low scattering power of the magadiite crystals, a structure analysis by conventional single crystal diffraction was not feasible. Instead, powder XRD data was recorded from a Siemens D5000 powder diffractometer in modified Debye-Scherrer geometry using Cu$K\alpha_1$ radiation (λ = 1.54059 Å). The diffractometer was equipped with a curved germanium (111) primary monochromator and a Braun linear position-sensitive detector (coverage = 6 °). The powder sample was sealed in a borosilicate glass capillary (with a diameter

of 0.3 mm) to avoid loss or uptake of water from the atmosphere. The structure model was refined using the FullProf 2K program (Rodríguez-Carvajal 1993) with default scattering factors. No absorption correction was necessary. Soft distance restraints were used for d(Si–O) = 1.610(5) Å, d(Si···Si) = 3.10(2) Å, d(O···O) = 2.63(2) Å.

Displacement parameters B_{iso} for crystal chemically similar atoms (e.g., the silicon atoms, the oxygen atoms of the silicate layer, the oxygen atoms representing water molecules) were constrained to remain equal. Additional parameters had to be used to account for the anisotropic halfwidth of reflections.

RESULTS AND DISCUSSION

General Characterization

The magadiite sample consists of very thin, colorless, intergrown crystals (Fig. 1 a). Individual plate-like crystals are approximately 1 μm–3 μm in diameter with a thickness of about 0.05 μm–0.1 μm (Fig. 1 b). The plates show a rectangular shape indicating an orthorhombic symmetry (Fig. 1 c). The SEM photographs showed no impurity phase. Qualitative chemical analysis confirmed the presence of sodium (Na), silicon (Si), oxygen (O) and a trace of iron (Fe).

DTA and TG curves of the thermal analysis of magadiite are presented in Fig. 2. The TG shows a significant weight loss which occurs in two major steps. The first weight loss starts at very low temperature (30 °C) indicating that a part of the water molecules are only loosely bonded within the structure. The first step between 40 °C–190 °C amounts to about 12.8 % and

represents the removal of structural water. The second step (190 °C–1200 °C) with a decrease in weight of around 3.6 % is due to the expulsion of water generated by a gradual condensation of silanol groups. After heating the sample up to 1200 °C, the remaining product is a mixture of tridymite and cristobalite.

The chemical composition as determined by AAS resulted in 74.0 wt% SiO_2, 5.1 wt% Na_2O and 0.3 wt% Fe_2O_3, 0.3 wt% Al_2O_3, 0.2 wt% K_2O and 0.2 wt% CaO (other elements were not analyzed) plus 16.4 wt% H_2O as determined by the TGA with a total sum of 96.5 wt%. Al, Fe, Ca and K are tentatively assigned to impurity phase(s) which, however, were not detected by XRD or SEM. The remaining mass (3.5 wt%) is assigned to additional water which was not registered by the TG analysis but already lost at room temperature in the dry air stream of the thermal analyzer. Ignoring the small content of Al, Fe, Ca and K, taking into account the silicon Q^4 to Q^3 ratio of 2.5 (^{29}Si NMR spectroscopy) and normalizing the silicon content to 14 Si per formula unit, the composition of the magadiite sample is: $Na_{1.9}[Si_{14}O_{28}(OH)_{2.4}]*10.2H_2O$.

The infrared spectrum of magadiite (Figs. 3 and 4) confirms the results of the TGA measurement concerning the composition of magadiite. The most prominent features of the spectrum are very broad and intense absorption bands around 3400 cm^{-1} (stretching vibrations) and two sharp bands around 1640 cm^{-1} (bending vibrations). These types of signals are typical for water molecules interconnected by hydrogen bonds of different strength. The characteristic pattern of the spectrum in the "water range" (1600 cm^{-1}–3800 cm^{-1}) is very similar to the one of synthetic Na-RUB-18 (see Fig. 3) suggesting that magadiite also contains bands of

interconnected [$Na(H_2O)_{6/1.5}$] octahedra in the inter-layer region and that the nature of the silanol groups of the silicate layer of magadiite may be similar to that of Na-RUB-18.

The bands in the region between 400 cm^{-1} and 1250 cm^{-1} (lattice vibrations, see Fig. 4) are, tentatively, assigned as follows: a very broad signal in the range of approximately 1150 cm^{-1}–950 cm^{-1}, with accentuated bands at 1070 cm^{-1}, 1060 cm^{-1} and 1021 cm^{-1} represents the asymmetric stretching vibration of Si–O–Si units. There is no band visible at around 960 cm^{-1} typical for stretching vibrations of terminal Si–OH groups, possibly because of a comparatively low amount of silanol groups and due to overlap with the broad signal at 1021 cm^{-1}. The bands at 812 cm^{-1} and 778 cm^{-1} are assigned to symmetric stretching vibrations of Si–O–Si units, whereas the band at 433 cm^{-1} represents the Si–O–Si bending vibrations (Y. Wang et al. 2009; Frost et al. 2013). Other signals at 706 cm^{-1} (weak), 615 cm^{-1} (strong), 576 cm^{-1} (strong) and 547 cm^{-1} (weak) cannot be assigned to specific units of the structure.

The ^{29}Si HPDEC MAS NMR spectrum (Fig. 5) shows four sharp signals which indicate that two types of Si environments exist in magadiite. The signal at δ = -98.8 ppm is assigned to Q^3-type silicon representing the terminal silanol (≡Si–OH) and/or siloxy (≡Si–O^-) groups of the silicate layer. The other three signals at -109.2, -111.0 and -113.5 ppm represent Q^4 type silicon, i.e., four-connected Si-units as in framework silicates. A fit of the ^{29}Si HPDEC MAS NMR spectrum yielded signal intensities as presented in Table 1. The total intensity ratio of the signals is Q^4 to Q^3 = 2.38 or, approximately 5 : 2.

Other synthetic magadiite samples are characterized by similar spectra: Typically, the ^{29}Si MAS NMR spectra – if sufficiently resolved – present four signals at about -99, -110, -111 and -113 ppm. The integrated intensity ratios of Q^4 to Q^3 signals in the literature, however, differ significantly with values between 1 and 3 (Garcés 1988; Pinnavaia et al. 1986). Q^4 to Q^3 ratios of 1 up to 1.5 are falsified when the pulse repetition time is too short (Scholzen et al. 1991). Other differences in values may possibly be explained by impure samples or partial condensation of silanol groups.

The ^{1}H spectrum (Fig. 6) displays two signals: a broad and intense one at 3.9 ppm attributed to the protons of the water molecules, and a weaker, but still distinct, signal at 15.2 ppm corresponding to strong hydrogen bonds with an O···O distance of about 2.5 Å (calculated according to Jeffrey et al., 1986 (Jeffrey and Yeon 1986); Eckert et al., 1988 (Eckert et al. 1988)). This distance correlates well with the distance between the terminal oxygen atoms of the silanol groups of the silicate layers as determined by the structure analysis (see below). Very similar ^{1}H MAS NMR spectra have been observed for synthetic magadiite (Krysiak et al., 2021) and structurally related kenyaite (Marler et al., 2021).

The X-ray powder diffraction diagram (see Fig. 7) presents a mixture of moderately sharp and broadened reflections. All reflections have been indexed based on an orthorhombic lattice with lattice parameters a_0 = 10.50 Å, b_0 = 10.03 Å and c_0 = 61.93 Å. The anisotropic peak broadening is related to specific (hkl) values. In particular, (hk0) and (00l) reflections possess the smallest halfwidths while (h0l), (0kl) and (hkl) reflections assume a broader shape. Although the plate-

like crystals are very thin (thickness of the crystals approximately 0.05 μm–0.1 μm along the c_0-axis), which should lead to some line broadening due to particle size, the (00l)-reflections are reasonably sharp. It can, therefore, be concluded that the thickness of all silicate layers and the distances between neighboring layers are identical throughout the crystal. The sharpness of (hk0)-reflections indicates that the structure is well ordered within the layer (ab-plane).

The analysis of the reflection conditions turned out to be difficult but led to the two most probable space group symmetries: *Fddd* and *F2dd*. The first strong peak of the powder diffraction diagram at d = 15.5 Å was assumed to represent the repeat unit of individual silicate layers along the stacking direction. Compared to synthetic magadiite samples, the natural material exhibits adequately sharp PXRD reflections indicative of a fairly well ordered structure (Fig. 8).

The results of the general characterization (thin plate like crystals, the presence of Q^3-type silicon and a powder diffraction pattern with a very strong reflection at a lower angle) were indicative of a layered silicate. The chemical analysis (Si to Na ratio ≈ 7), the unit cell parameter $c_0 \approx 62$ Å and the silicon Q^4 to Q^3 ratio ≈ 2.5 hinted toward a rather thick silicate layer. Insights from FT-IR spectroscopy suggested that the inter-layer region of Na-RUB-18 and magadiite may be structurally related.

Structure analysis

Structure determination

The crystal structure was solved from small synthetic magadiite crystals of limited crystallinity in a complex process using 3D electron diffraction (3D ED) combined with model building (Krysiak 2018; Krysiak et al. 2021). Knowing/assuming that the structure of magadiite possesses i) thick silicate layers, ii) relatively few terminal silanol/siloxy groups iii) an inter-layer region containing bands of edge-sharing $[Na(H_2O)_{6/1.5}]$ octahedra as present in Na-RUB-18, iv) only one sodium site, and v) space group symmetry *Fddd* (first guess), the obtained electron density maxima of the Fourier map could be assigned to a partial structure including most of the silicon and oxygen sites and the sodium site. Subsequently, this partial structure model was completed by geometrical considerations (tetrahedrally coordinated silicon atoms, Si–O bond distances of about 1.6 Å, Si–O–Si angles of approximately 150 °, the presence of some silanol groups) and by adding the missing water molecules in accordance with the Na-RUB-18 structure. To obtain a completely coherent structure model, the space group had to be reduced to *F2dd*. For a better comparison with related structures, a specific unit cell setting was chosen that led to *F2dd* instead of standard setting *Fdd2* (No. 43).

Structure refinement

Assuming space group symmetry *F2dd* to be correct, the structure model contains 32 Q^3-type and 80 Q^4-type Si atoms per unit cell which would approximately concur with the ^{29}Si NMR

344 spectrum presenting a Q^3 to Q^4 intensity ratio of around 1 : 2.4. This structure model was
345 sufficient to start the Rietveld refinement based on the X-ray powder diffraction data.

346 Since even the relatively sharp reflections of magadiite exhibit halfwidths two times larger
347 (approximately 0.17 °2θ at around 24 °2θ) than those of highly crystalline material (e.g., quartz
348 with approximately 0.08 °2θ), it is suggested that the real structure of natural magadiite shows a
349 deviation from a strictly regular layer stacking along [001] with slight shifts in the [100] and/or
350 [010] direction. This is characteristic of hydrated layer silicates having only weak bonding
351 interactions between neighboring silicate layers (Marler and Gies 2012). The real structure and
352 the nature of the disorder, however, will be analyzed in a future study.

353 The refinement of the initial structure model was performed assuming space group symmetry
354 *F2dd* (no. 43). The details of data collection and the results of the structure refinement are
355 summarized in Table S1 of the supplemental file. The refinement in space group *F2dd* converged
356 to residual values $R_{Bragg} = 0.031$ and $R_F = 0.026$ confirming the structure model (see Fig. 9 for
357 the Rietveld plot). It was, nevertheless, not possible to account for the anisotropic broadening of
358 the peaks in a complete fashion. The profile fit is, thus, not as good as usually obtained with a
359 more-ordered material ($\chi^2 = 8.5$). The physico-chemical characterization using solid-state NMR
360 spectroscopy, SEM, TG-DTA, and DRIFT spectroscopy as discussed before confirms the
361 correctness of the structure model.

362

Description of the structure

The unit cell content of magadiite, according to structure analysis, chemical analysis, TG and NMR spectra, is $Na_{16}[Si_{112}O_{224}(OH)_{16}]*64H_2O$, or $Na_2[Si_{14}O_{28}(OH)_2]*8H_2O$ for a better comparison with compositions presented in the literature.

The unit cell contains four silicate layers stacked along the c_0-axis with a sequence of ABA'B' (Fig. 10 left). Two neighboring layers are always mirror images of each other, generating left-handed layer A and right-handed layer B. When stacking the layers, a successive layer is always shifted by $+¼*c_0$ relative to the subjacent layer. In addition, layer B is shifted relative to starting layer A along [110] by a quarter of this diagonal (≈ 3.6 Å). The next layer A' is shifted relative to B along [1-10] by, again, 3.6 Å; the following layer B' is shifted relative to A' along [-1-10] by the same value, and, finally, layer A is shifted relative to B' along [-110] by ≈ 3.6 Å. This manner of stacking leads to a pseudo 4_1 screw axis along c_0.

The two layers A and B are enantiomers and represent silicate layers (Fig. 11) of so-far-unknown topology. Seven symmetrically independent silicon and 15 independent oxygen sites are present, forming a dense layer of considerable thickness (11.5 Å). The dense layers exhibit neither a porosity along [001] nor micro-channels within the layer (see Fig. 11). Both layers possess a thickness of 11.5 Å (without van der Waals radii of the terminal oxygen atoms) and a silicon Q^4 to Q^3 ratio of 2.5. The silicate layers of magadiite display a complex structure constructed from 4-, 5-, 6-, and 7-rings. Distances between atoms vary in the ranges: d(Si–O) = 1.57 Å–1.65 Å, d(Si···Si) = 2.99 Å–3.21 Å, d(O···O) = 2.49 Å–2.75 Å. Atomic coordinates, displacement parameters and occupancy factors are presented in Table S2.

384 The layers are terminated by silanol (≡Si–OH) and siloxy (Si–O^-) groups. 16 out of 32
385 terminal Si–O groups per unit cell are protonated, the remaining groups compensate the charge
386 of the sodium cations. The corresponding oxygen atoms feature a short distance between each
387 other, d(OH···OH) = 2.47 Å, indicating a strong intra-layer hydrogen bond which is in
388 agreement with the ^{1}H MAS NMR signal at 15.2 ppm (see Fig. 6 and corresponding text). Strong
389 intra-layer hydrogen bonds with O···O distances as short as 2.3 Å have been observed already in
390 several HLSs depending on the particular topology of the silicate layer (see Table 3 in Marler
391 and Gies 2012). In order to distinguish the silicate layer of magadiite from other layer types of
392 HLSs (Marler et al. 2021), the acronym "mag layer" is proposed in accordance to other, so far
393 classified layer types.

394 The structure of magadiite is completed by bands of interconnected [$Na(H_2O)_{6/1.5}$] octahedra
395 intercalated between neighboring silicate layers and extending along [110] at z ≈ 0.125 and [1-
396 10] at z ≈ 0.375. Na···O distances of the distorted octahedra vary between 2.23 Å–2.77 Å
397 (distances have not been restrained during refinement). To include the scattering power of the
398 hydrogen atoms which were not traceable, the occupancy factor of the oxygen atoms
399 representing the water molecules was increased by a factor of 1.25. Four different water sites
400 exist in the inter-layer region, whereas the [$Na(H_2O)_{6/1.5}$] octahedra are partially distorted. This
401 distortion, however, may be an artifact due to the slight disorder of the structure. Distances
402 between the oxygen atoms representing the water molecules vary in the range of 3.34 Å–3.76 Å
403 forming very weak hydrogen bonds with each other.

404 The water molecules OW3 and OW4 are hydrogen bonded to terminal silanol groups with
405 O···O distances of 2.54 Å–2.91 Å (Fig. 11). The surface zone of the silicate layers, as well as the
406 inter-layer region containing the $[Na(H_2O)_{6/1.5}]$ octahedra, are closely related to Na-RUB-18,
407 $Na_2[Si_{10}O_{18}(OH)_6]$. Fig. 12 presents a comparison of the two related structures. Chemically,
408 magadiite is related to the sodium layer silicates Na-RUB-18/octosilicate; kanemite,
409 $Na_4[Si_8O_{16}(OH)_4]*12H_2O$ (Garvie et al. 1999; Vortmann et al. 1999); makatite,
410 $Na_8[Si_{16}O_{32}(OH)_8]*16H_2O$ (Annehed et al. 1982); and kenyaite, $Na_2Si_{20}O_{41}*xH_2O$ (Beneke and
411 Lagaly 1983; Marler et al., 2021).

412

413 Magadiite shows evidence of minor structural disorder typical for HLSs which, generally,
414 exhibit weak interactions between neighboring layers. In this respect, the result of the structure
415 refinement represents an idealized structure. Nonetheless, the magadiite mineral possesses a
416 considerably higher degree of structural order than any synthetic magadiite sample available to
417 us. The structure as obtained by the Rietveld refinement reveals the general features of the
418 magadiite structure, such as topology of the silicate layer, as well as the presence and the
419 location of the mutually interconnected $[Na(H_2O)_{6/1.5}]$ octahedra intercalated between the silicate
420 layers. Precise bond lengths and bond angles, however, cannot be derived from this structure
421 analysis because of the disorder. This will be the subject of further research on the detailed
422 analysis of the "real structure".

423

Hypothetical framework structure of condensed magadiite

It is well known that HLS can be transformed into zeolite materials possessing microporous frameworks. The silicate layers can formally be condensed by a reaction ≡Si–OH + HO–Si≡ → ≡Si–O–Si≡ + H_2O to generate a framework structure. This has been demonstrated in the successful condensation of, e.g., RUB-15 to silica sodalite (Moteki et al. 2011), β-helix layered silicate to AST type zeolite, (Asakura et al. 2014), PREFER to silica ferrierite (Schreyeck et al. 1996), layer silicate RUB-18 to a zeolite of the RWR type (Marler et al. 2005; Oumi et al. 2007; Ikeda et al. 2008) and RUB-39 to RUB-41 (= RRO type zeolite) (Y. Wang et al., 2005).

So far, only disordered structures of condensed magadiite have been obtained. In 2008, Oumi et al. (Oumi et al. 2008) presented a most promising approach to convert magadiite into a microporous silica material via an intercalation of acetic acid molecules and TMA^+ cations into the inter-layer region of magadiite. The intercalation of TMA^+ cations and AcOH molecules induced an improvement in the configuration of the silanol groups. The resulting Ac-magadiite and Ac-TMA-magadiite were calcined to form a microporous material with an average pore diameter of 0.55 nm by dehydration-condensation of the silanol groups. Later, Asakura et al. presented a study on the condensation of protonated magadiite through refluxing in N-methylformamide (Asakura et al. 2015).

Although microporous materials were in fact obtained from magadiite, the quality of the XRD powder diagrams of the materials is poor, showing only few broad reflections indicative of severe disorder. Consequently, no structure models of the microporous framework silicate were presented.

In order to mutually interconnect all silanol groups of neighboring layers, adjacent layers have merely to be shifted along c_0. No shift relative to the a_0 and b_0 axes is necessary for a common approach. This formal condensation would generate a new zeolite framework type possessing 8-ring channels running along [110] and [1-10]. The corresponding c_0 value would decrease from 61.95 Å to approximately 45.00 Å (DLS refinement, see below) generating a quite dense structure with a calculated framework density of 21.5 T/1000 $Å^3$. This framework density is higher than the densities of all known pure silica zeolites as listed in the Database of Zeolite Structures (Baerlocher and McCusker 2017). The silica zeolite with the highest density, so far, is NU-6(2) with FD = 21.0. Condensed magadiite, therefore, may be useful as an all-silica zeolite being thermally stable up to a temperature of at least 1000°C.

To conclude the condensation into a complete, non-interrupted framework, the removal of Na^+ ions by an ion exchange against, e.g., protons, is imperative in order to avoid charge compensating defects (≡Si–O^-···HO–Si≡) in the framework. A replacement of the Na^+ ions by organic cations of suitable size and geometry might rearrange the layer stacking of magadiite into a completely ordered sequence and might also, subsequently, yield an ordered framework by condensation.

The hypothetical framework structure of condensed magadiite in its ordered form is shown in Figure 10 on the right. Corresponding atomic coordinates as obtained by a DLS refinement are listed in Table 2. The DLS refinement resulted in an exceedingly good *R*-factor of 0.0050% indicating that this type of framework topology can be constructed as a silica modification with undistorted angles and ideal bond lengths. The simultaneous refinement of the lattice parameters

This is the peer-reviewed, final accepted version for American Mineralogist, published by the Mineralogical Society of America.
The published version is subject to change. Cite as Authors (Year) Title. American Mineralogist, in press.
DOI: https://doi.org/10.2138/am-2022-8156. http://www.minsocam.org/

generated a_0 = 10.7280 Å, b_0 = 10.7863 Å, c_0 = 45.0046 Å. Figure 13 displays the simulated X-ray powder diffraction pattern (CuKα_1 radiation) of the DLS refined structure. It is characterized by a first strong reflection at 7.9 °2θ (d = 11.25 Å) and two groups of medium strong reflections in the ranges of 12 °2θ–16 °2θ and 23 °2θ–28 °2θ. This pattern can be compared to the one of a real material, calcined (condensed) magadiite which had previously been treated with N-methylformamide, (see Fig. 1e in Asakura et al. (Asakura et al. 2015)). The experimental pattern, as well, shows a strong reflection at d = 11 Å and two groups of medium strong reflections at 12 °2θ–16 °2θ and 23 °2θ–28 °2θ. The reflections, however, are broad, indicating severe disorder.

IMPLICATIONS

The structural characterization of hydrous layer silicates (layered alkali silicates) is a most important task in order to realize the complex nature of these materials. A minor disorder concerning layer arrangement or layer structure contributes to the diffraction diagram of magadiite rendering the interpretation and understanding complicated. Nevertheless, exploiting the additional information of this contribution, it was possible to solve the structure of a mineral, which was concealed for more than 50 years. As can be learned from a comparison of the Rietveld refinements of natural (this study) and synthetic magadiite (Krysiak et al. 2021), the topologies of the dense silicate layers are identical. In general, however, the natural magadiite possesses better structural order. This becomes evident in comparing the FWHM of the diffraction peaks of natural magadiite, 0.17-0.47 (this study, Table S1) with that of synthetic magadiite, 0.28-0.73 (Krysiak et al. 2021, Suppl. Table 3). Also, the estimated standard

487 deviations of the refined atomic coordinates of natural magadiite are approximately 20 percent
488 smaller compared to those of synthetic magadiite.

489 Magadiite analogues are frequently synthesized in numerous laboratories and are utilized to
490 produce new porous materials. For the future development of improved materials, the knowledge
491 of the structure of magadiite is fundamental. The detailed information of the inter-layer space in
492 geometry and composition allows for the specific operation to modify the layered precursor. This
493 might be ion exchange, transformation in the acidic form, adsorption of organics etc. Using
494 (topotactic) condensation reaction, pillaring or grafting treatments, new materials with new
495 properties will be obtained which are otherwise not accessible.

496

497 ## ACKNOWLEDGEMENTS

498 The authors are very grateful to K. Beneke and Prof. Dr. G. Lagaly, Kiel, Germany, for kindly
499 providing natural magadiite samples. Also, many thanks to K. Kuroda and M. Koike, Tokyo,
500 Japan, for suggestions regarding the structure solution. Moreover, the authors thank
501 S. Grabowski for recording the NMR spectra. The work was funded by the Deutsche
502 Forschungsgemeinschaft with grant number MA 6641/3-1. Yaşar Krysiak is very grateful for the
503 support by the Czech Science Foundation, project number 19-08032S.

504

REFERENCES

Almond, G.G., Harris, R.K., Franklin, K.R., and Graham, P. (1996) A ^{23}Na NMR study of hydrous layered silicates. Journal of Materials Chemistry, 6, 843–847.

Annehed, H., Faelth, L., and Lincoln, L.J. (1982) Crystal structure of synthetic makatite $Na_2Si_4O_8(OH)_{2.4}H_2O$. Zeitschrift für Kristallographie, 159, 203–210.

Anthony, J.W., Bideaux, R.A., Bladh, K.W., and Nichols, M.C. (2003) Handbook of mineralogy: Online version. (J.W. Anthony, R.A. Bideaux, K.W. Bladh, & M.C. Nichols, Eds.).

Asakura, Y., Takayama, R., Shibue, T., and Kuroda, K. (2014) Topotactic conversion of β-helix-layered silicate into AST-type zeolite through successive interlayer modifications. Chemistry - A European Journal, 20, 1893–1900.

Asakura, Y., Hosaka, N., Osada, S., Terasawa, T., Shimojima, A., and Kuroda, K. (2015) Interlayer condensation of protonated layered silicate magadiite through refluxing in N-methylformamide. Bulletin of the Chemical Society of Japan, 88, 1241–1249.

Baerlocher, C., and McCusker, L.B. (2017) Database of zeolite structures.

Baerlocher, C., Hepp, A., and Meier, W.M. (1978) DLS-76, a FORTRAN program for the simulation of crystal structures by geometric refinement. ETH, Zürich, Zürich, Switzerland.

Beneke, K., and Lagaly, G. (1983) Kenyaite - synthesis and properties. American Mineralogist, 68, 818–826.

524 Brandt, A., Schwieger, N., and Bergk, K.-H. (1987) A new model structure of sheet sodium
525 (Na) silicate hydrates (Na-SH) - theoretical view based on known X-ray and NMR-
526 measurements. In P. Gauthier-Villars, Ed., Revue de Chimie Minérale Vol. 24, pp. 564–571.

527 Brandt, A., Schwieger, W., and Bergk, K.-H. (1988) Development of a model structure for the
528 sheet silicate hydrates ilerite, magadiite, and kenyaite. Crystal Research and Technology, 23,
529 1201–1203.

530 Brandt, A., Schwieger, W., Bergk, K.-H., Grabner, P., and Porsch, M. (1989) Structure and
531 properties of Na-magadiite dependent on temperature. Crystal Research and Technology, 24, 47–
532 54.

533 Brindley, G.W. (1969) Unit cell of magadiite in air, in vacuo, and under other conditions.
534 American Mineralogist, 54, 1583–1591.

535 Doustkhah, E., and Ide, Y. (2020) Microporous layered silicates: Old but new microporous
536 materials. New Journal of Chemistry, accepted.

537 Eckert, H., Yesinowski, J.P., Silver, L.A., and Stolper, E.M. (1988) Water in silicate glasses:
538 Quantitation and structural studies by proton solid echo and magic angle spinning NMR
539 methods. The Journal of Physical Chemistry, 92, 2055–2064.

540 Eugster, H.P. (1967) Hydrous sodium silicates from lake magadi, kenya: Precursors of bedded
541 chert. Science, 157, 1177–1180.

542 ——— (1969) Inorganic bedded cherts from the magadi area, kenya. Contributions to
543 Mineralogy and Petrology, 22, 1–31.

Feng, F., and Balkus, K.J., Jr. (2003) Synthesis of kenyaite, magadiite and octosilicate using poly(ethylene glycol) as a template. Journal of Porous Materials, 10, 5–15.

Frost, R.L., Xi, Y., Scholz, R., Lopez, A., and Belotti, F.M. (2013) Infrared and Raman spectroscopic characterization of the silicate-carbonate mineral carletonite - $KNa_4Ca_4Si_8O_{18}(CO_3)_4(OH,F)*H_2O$. Journal of Molecular Structure, 1042, 1–7.

Garcés, J.M. (1988) Hypothetical structures of magadiite and sodium octosilicate and structural relationships between the layered alkali metal silicates and the mordenite- and pentasil-group Zeolites. Clays and Clay Minerals, 36, 409–418.

Garvie, L.A.J., Devouard, B., Groy, T.L., Camara, F., and Buseck, P.R. (1999) Crystal structure of kanemite, $NaHSi_2O_5*3H_2O$, from the aris phonolite, namibia. American Mineralogist, 84, 1170–1175.

Gies, H., Marler, B., Vortmann, S., Oberhagemann, U., Bayat, P., Krink, K., Rius, J., Wolf, I., and Fyfe, C.A. (1998) New structures—new insights: Progress in structure analysis of nanoporous materials. Microporous and Mesoporous Materials, 21, 183–197.

Horváth, L., and Gault, R.A. (1990) The mineralogy of mont saint-hilaire, quebec. The Mineralogical Record, 21, 284–359.

Huang, Y., Jiang, Z., and Schwieger, W. (1999) Vibrational spectroscopic studies of layered silicates. Chemistry of Materials, 11, 1210–1217.

Hudson Institute of Mineralogy (1993-20201993-2020) Magadiite: mindat.org. (https://www.mindat.org/min-2530.html, accessed May 10, 2021).

564 Ide, Y., Tominaka, S., Kono, H., Ram, R., Machida, A., and Tsunoji, N. (2018) Zeolitic
565 intralayer microchannels of magadiite, a natural layered silicate, to boost green organic
566 synthesis. Chemical Science, 9, 8637–8643.

567 Ikeda, T., Oumi, Y., Takeoka, T., Yokoyama, T., Sano, T., and Hanaoka, T. (2008)
568 Preparation and crystal structure of RUB-18 modified for synthesis of zeolite RWR by topotactic
569 conversion. Microporous and Mesoporous Materials, 110, 488–500.

570 Jeffrey, G.A., and Yeon, Y. (1986) The correlation between hydrogen-bond lengths and
571 proton chemical shifts in crystals. Acta Crystallographica Section B: Structural Science, 42, 410–
572 413.

573 Jones, B.F., Rettig, S.L., and Eugster, H.P. (1967) Silica in alkaline brines. Science, 158,
574 1310–1314.

575 Kim, C.S., Yates, D.M., and Heaney, P.J. (1997) The layered sodium silicate magadiite: An
576 analog to smectite for benzene sorption from water. Clays and Clay Minerals, 45, 881–885.

577 Kim, S.J., Kim, M.H., Seo, G., and Uh, Y.S. (2012) Preparation of tantalum-pillared
578 magadiite and its catalytic performance in Beckmann rearrangement. Research on Chemical
579 Intermediates, 38, 1181–1190.

580 Krysiak, Y. (2018) Unordnung im Nanobereich: Schichtstrukturen unter dem
581 Elektronenmikroskop. Dissertation, Johannes Gutenberg-University Mainz, Mainz, Germany.

582 Krysiak, Y., Maslyk, M., Silva, B.N., Plana-Ruiz, S., Moura, H.M., Munsignatti, E.O., Vaiss,
583 V.S., Kolb, U., Tremel, W., Palatinus, L., Leitão, A.A., Marler, B. and Pastore, H.O. (2021) The

584 elusive structure of magadiite, solved by 3D electron diffraction and model building. Chem.
585 Mater., 33, 9, 3207–3219.

586 Kuroda, K. (1996) Silica-based mesoporous molecular sieves derived from a layered
587 polysilicate kanemite - a review. Journal of Porous Materials, 3, 107–114.

588 Lagaly, G. (1986) Interaction of alkylamines with different types of layered compounds. Solid
589 State Ionics, 22, 43–51.

590 Lagaly, G., Beneke, K., and Weiss, A. (1975) Magadiite and H-magadiite: II. H-magadiite
591 and its intercalation compounds compounds. American Mineralogist, 60, 650–658.

592 Maglione, G.F. (1970) La magadiite, silicate sodique de néoformation des faciès
593 évaporitiques du kanem (littoral nord-est du lac tchad): Magadiite, an authentic sodic silicate of
594 the evaporite facies in kanem, northeast shore of lake chad. Bulletin Du Service de La Carte
595 géologique d'Alsace Et de Lorraine, 23, 177–190.

596 Marler, B., and Gies, H. (2012) Hydrous layer silicates as precursors for zeolites obtained
597 through topotactic condensation: A review. European Journal of Mineralogy, 24, 405–428.

598 Marler, B., Ströter, N., and Gies, H. (2005) The structure of the new pure silica zeolite RUB-
599 24, $Si_{32}O_{64}$, obtained by topotactic condensation of the intercalated layer silicate RUB-18.
600 Microporous and Mesoporous Materials, 83, 201–211.

601 Marler, B., Grünewald-Lüke, A., Ikeda, T., and Gies, H. (2021) Database of hydrous layer
602 silicates. (https://hls-database.com, accessed May 10, 2021).

603 Marler, B., Grosskreuz, I., Gies, H. (2021), The crystal structure of synthetic kenyaite,
604 $Na_2Si_{20}O_{40}(OH)_2*8H_2O$. Journal of Solid State Chemistry, article in press.

605 McAtee, J.L., House, R., and Eugster, H.P. (1968) Magadiite from Trinity County, California.
606 American Mineralogist, 53, 2061–2069.

607 Moteki, T., Chaikittisilp, W., Sakamoto, Y., Shimojima, A., and Okubo, T. (2011) Role of
608 acidic pretreatment of layered silicate RUB-15 in its topotactic conversion into pure silica
609 sodalite. Chemistry of Materials, 23, 3564–3570.

610 Ogawa, M., and Kuroda, K. (1997) Preparation of inorganic-organic nanocomposites through
611 intercalation of organoammonium ions into layered silicates. Bulletin of the Chemical Society of
612 Japan, 70, 2593–2618.

613 Ogawa, M., and Maeda, N. (1998) Intercalation of tris(2,2'-bipyridine)ruthenium(II) into
614 magadiite. Clay Minerals, 33, 643–650.

615 Ogawa, M., Yamamoto, M., and Kuroda, K. (2001a) Intercalation of an amphiphilic
616 azobenzene derivative into the interlayer space of a layered silicate, magadiite. Clay Minerals,
617 36, 263–266.

618 Ogawa, M., Ishii, T., Miyamoto, N., and Kuroda, K. (2001b) Photocontrol of the basal
619 spacing of azobenzene-magadiite intercalation compound. Advanced Materials, 13, 1107–1109.

620 Oumi, Y., Takeoka, T., Ikeda, T., Yokoyama, T., and Sano, T. (2007) Convenient conversion
621 of crystalline layered silicate octosilicate into RWR-type zeolite by acetic acid intercalation.
622 New Journal of Chemistry, 31, 593–597.

623 Oumi, Y., Takagi, K., Ikeda, T., Sasaki, H., Yokoyama, T., and Sano, T. (2008) Structural
624 conversion of crystalline layered silicate magadiite to microporous material by acetic acid
625 intercalation. Journal of Porous Materials, 16, 641.

626 Pinnavaia, T.J., Johnson, I.D., and Lipsicas, M. (1986) A ^{29}Si MAS NMR study of tetrahedral
627 site distributions in the layered silicic acid H^+-magadiite ($H_2Si_{14}O_{29}*nH_2O$) and in Na^+-magadiite
628 ($Na_2Si_{14}O_{29}*nH_2O$). Journal of Solid State Chemistry, 63, 118–121.

629 Rammlmair, D., Ed. (2000) Applied mineralogy: In research, economy, technology, ecology
630 and culture ; proceedings of the sixth international congress on applied mineralogy ICAM 2000,
631 Göttingen, Germany, 17 - 19 July 2000. Balkema, Rotterdam.

632 Rodríguez-Carvajal, J. (1993) Recent advances in magnetic structure determination by
633 neutron powder diffraction. Physica B: Condensed Matter, 192, 55–69.

634 Rooney, T.P., Jones, B.F., and Neal, J.T. (1969) Magadiite from Alkali Lake, Oregon.
635 American Mineralogist, 54, 1034–1043.

636 Roth, W.J., Gil, B., Makowski, W., Marszalek, B., and Eliášová, P. (2016) Layer like porous
637 materials with hierarchical structure. Chemical Society Reviews, 45, 3400–3438.

638 Ruiz-Hitzky, E., Rojo, J.M., and Lagaly, G. (1985) Mechanism of the grafting of
639 organosilanes on mineral surfaces. Colloid and Polymer Science, 263, 1025–1030.

Sassi, M., Miehé-Brendlé, J., Patarin, J., and Bengueddach, A. (2005) Na-magadiite prepared in a water/alcohol medium: Synthesis, characterization and use as a host material to prepare alkyltrimethylammonium- and Si-pillared derivates. Clay Minerals, 40, 369–378.

Scholzen, G., Beneke, K., and Lagaly, G. (1991) Diversity of magadiite. Zeitschrift für Anorganische und Allgemeine Chemie, 597, 183–196.

Schreyeck, L., Caullet, P., Mougenel, J.C., Guth, J.L., and Marler, B. (1996) PREFER: A new layered (alumino) silicate precursor of FER-type zeolite. Microporous Materials, 6, 259–271.

Schwieger, W., and Lagaly, G. (2004) Handbook of layered materials: Alkali silicates and crystalline silicic acids: (S. M. Auerbach, k. A. Carrado, p. K. Dutta, eds.). M. Dekker, New York.

Schwieger, W., Heidemann, D., and Bergk, K.-H. (1985) High-resolution solid-state ^{29}Si nuclear-magnetic-resonance spectroscopic studies of synthetic sodium-silicate hydrates. Revue de Chimie Minérale, 22, 639–650.

Shi, Z., Wang, Y., Meng, C., and Liu, X. (2013) Hydrothermal conversion of magadiite into mordenite in the presence of cyclohexylamine. Microporous and Mesoporous Materials, 176, 155–161.

Sirinakorn, T., Imwiset, K., Bureekaew, S., and Ogawa, M. (2018) Inorganic modification of layered silicates toward functional inorganic-inorganic hybrids. Applied Clay Science, 153, 187–197.

Sprung, R., Davis, M.E., Kauffman, J.S., and Dybowski, C. (1990) Pillaring of magadiite with silicate species. Industrial & Engineering Chemistry Research, 29, 213–220.

Superti, G.B., Oliveira, E.C., Pastore, H.O., Bordo, A., Bisio, C., and Marchese, L. (2007) Aluminum magadiite: An acid solid layered material. Chemistry of Materials, 19, 4300–4315.

Takahashi, N., and Kuroda, K. (2011) Materials design of layered silicates through covalent modification of interlayer surfaces. Journal of Materials Chemistry, 21, 14336–14353.

Vieira, R.B., and Pastore, H.O. (2014) Polyethylenimine-magadiite layered silicate sorbent for CO_2 capture. Environmental Science & Technology, 48, 2472–2480.

Vortmann, S., Rius, J., Siegmann, S., and Gies, H. (1997) Ab initio structure solution from X-ray powder data at moderate resolution: Crystal structure of a microporous layer silicate. The Journal of Physical Chemistry B, 101, 1292–1297.

Vortmann, S., Rius, J., Marler, B., and Gies, H. (1999) Structure solution from powder data of the hydrous layer silicate kanemite, a precursor of the industrial ion exchanger SKS-6. European Journal of Mineralogy, 11, 125–134.

Wang, Y., Shang, Y., Zhu, J., Wu, J., Ji, S., and Meng, C. (2009) Synthesis of magadiite using a natural diatomite material. Journal of Chemical Technology and Biotechnology, 84, 1894–1898.

Wang, Y., Lv, T., Wang, H., Zhao, Y., Meng, C., and Liu, H. (2015) ZSM-5 and ferrierite synthesized by magadiite conversion method in 1, 6-hexamethylenediamine system. Microporous and Mesoporous Materials, C, 66–71.

679 Wang, Y., Marler, B., Gies, H., Müller, U. (2005) Synthesis and crystal structure of zeolite
680 RUB-41 obtained as calcination product of a layered precursor: a systematic approach to a new
681 synthesis route. Chemistry of Materials, 17, 43-49.

682 Wang, Z., and Pinnavaia, T.J. (1998) Hybrid organic-inorganic nanocomposites: Exfoliation
683 of magadiite nanolayers in an elastomeric epoxy polymer. Chemistry of Materials, 10, 1820–
684 1826.

685 ## Tables

686

687 *Table 1: Results of the fit applied to the ^{29}Si HPDEC MAS NMR spectrum.*

No.	shift value	Type of Si	peak area	rel. no. of Si
1	−98.82 ppm	Q^3	29.6 %	2 Si
2	−109.24 ppm	Q^4	30.3 %	2 Si
3	−111.00 ppm	Q^4	26.6 %	2 Si
4	−113.54 ppm	Q^4	13.6 %	1 Si

688

This is the peer-reviewed, final accepted version for American Mineralogist, published by the Mineralogical Society of America.
The published version is subject to change. Cite as Authors (Year) Title. American Mineralogist, in press.
DOI: https://doi.org/10.2138/am-2022-8156. http://www.minsocam.org/

689 *Table 2: Atomic coordinates of the structure model of condensed magadiite derived by Distance-*

690 *least-squares refinement.*

atom	Wyckoff	x	y	z	occ. factor
Si1	16b	0.37580	0.75052	0.00152	11.0
Si2	16b	0.24501	0.91638	0.95356	11.0
Si3	16b	0.04018	0.12036	0.95226	11.0
Si4	16b	0.49245	0.06098	0.95385	11.0
Si5	16b	0.68931	0.86329	0.95208	11.0
Si6	16b	0.34131	0.50700	0.83960	11.0
Si7	16b	0.63397	0.21317	0.84091	11.0
O1	16b	0.12901	1.00579	0.96119	11.0
O2	16b	0.28285	0.83556	0.98223	11.0
O3	16b	0.94857	0.07906	0.92563	11.0
O4	16b	0.29536	0.66465	0.02362	11.0
O5	16b	0.56075	0.87416	0.07405	11.0
O6	16b	0.58364	0.95296	0.96596	11.0
O7	16b	0.46753	0.16182	0.97947	11.0
O8	16b	0.75037	0.93359	0.92395	11.0
O9	16b	0.45745	0.33774	0.01970	11.0
O10	16b	0.20637	0.17647	0.07298	11.0
O11	16b	0.36253	0.99965	0.94355	11.0
O12	16b	0.12522	0.23542	0.94166	11.0
O13	16b	0.71961	0.09261	0.83594	11.0
O20	16b	0.62120	0.23960	0.87579	11.0

691

Figure Captions

Figure 1: SEM photographs of magadiite.

Figure 2: DTA (upper, blue) and TG (lower, green) curves of magadiite. Two main steps can be distinguished: a) release of structural water between 40 °C–190 °C, b) expulsion of water through the condensation of the silicate between about 190 °C–1200 °C.

Figure 3: Comparison of the infrared spectra of Na-RUB-18 (red) and magadiite (blue) in the range of 1500 cm^{-1}–4000 cm^{-1} showing bands related to OH groups and water.

Figure 4: Infrared spectrum of magadiite in the region between 400 cm^{-1}–1300 cm^{-1} (lattice vibrations).

Figure 5: ^{29}Si MAS NMR spectrum of magadiite (black) and simulated spectrum (red).

Figure 6: ^{1}H MAS NMR spectrum of magadiite with spinning side bands (*) of the main signal.

Figure 7: Section of the XRD powder pattern of natural magadiite showing the anisotropic halfwidths of the reflections with corresponding Bragg reflections (red).

Figure 8: Comparison of XRD powder patterns of typical synthetic magadiite (a, bottom, green), synthetic magadiite of highest possible structural order (b, middle, red) and natural magadiite (c, top, blue).

Figure 9: Plot of the diffraction patterns after Rietveld analysis of magadiite. Experimental and calculated data are in the upper trace, and the difference plot is shown below. Tick marks for allowed reflections are given.

711 Figure 10: (left) The structure of magadiite projected on (110) showing the composite nature of
712 the material; (right) Hypothetical framework structure of condensed magadiite after removing
713 the intercalated bands of interconnected [$Na(H_2O)_{6/1.5}$] octahedra.

714 Figure 11: Schematic drawing of the structures of the silicate layers of magadiite in different
715 projections. Bridging oxygen atoms are omitted for clarity. Si: purple, OH: dark blue.

716 Figure 12: Details of the structure of magadiite showing the hydrogen bonds (light blue) between
717 water molecules WO3 and WO4 (light blue) and the oxygen atoms of the terminal silanol groups
718 (dark blue).

719 Figure 13: Structural relationship between the structures of magadiite (left) and Na-RUB-18
720 (right).

721 Figure 14: Distance-least-squares refinement of the lattice parameters of the hypothetical
722 framework structure of condensed magadiite.

Figure 1a

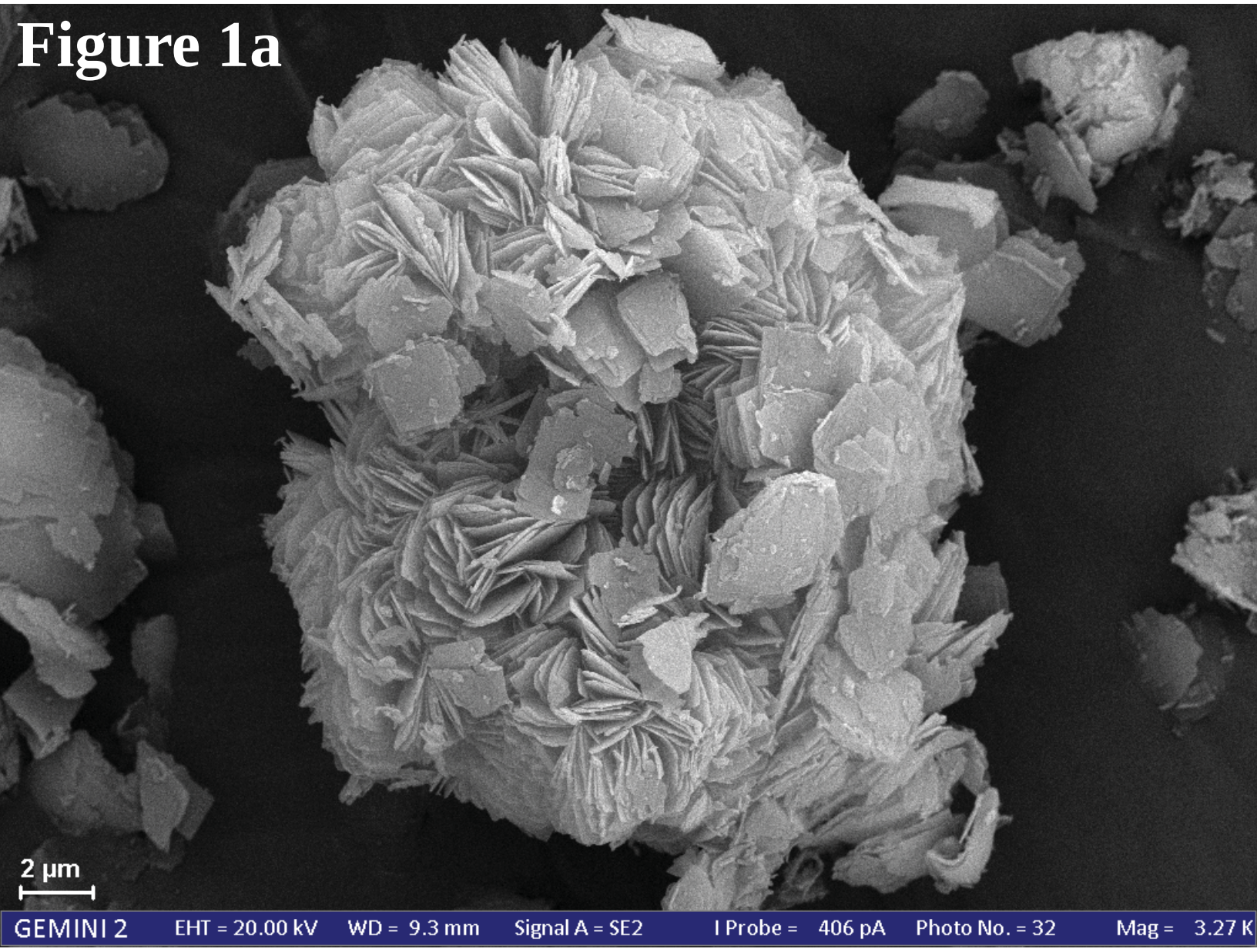
2 µm
GEMINI 2
EHT = 20.00 kV
WD = 9.3 mm
Signal A = SE2
I Probe = 406 pA
Photo No. = 32
Mag = 3.27 K

Figure 1b

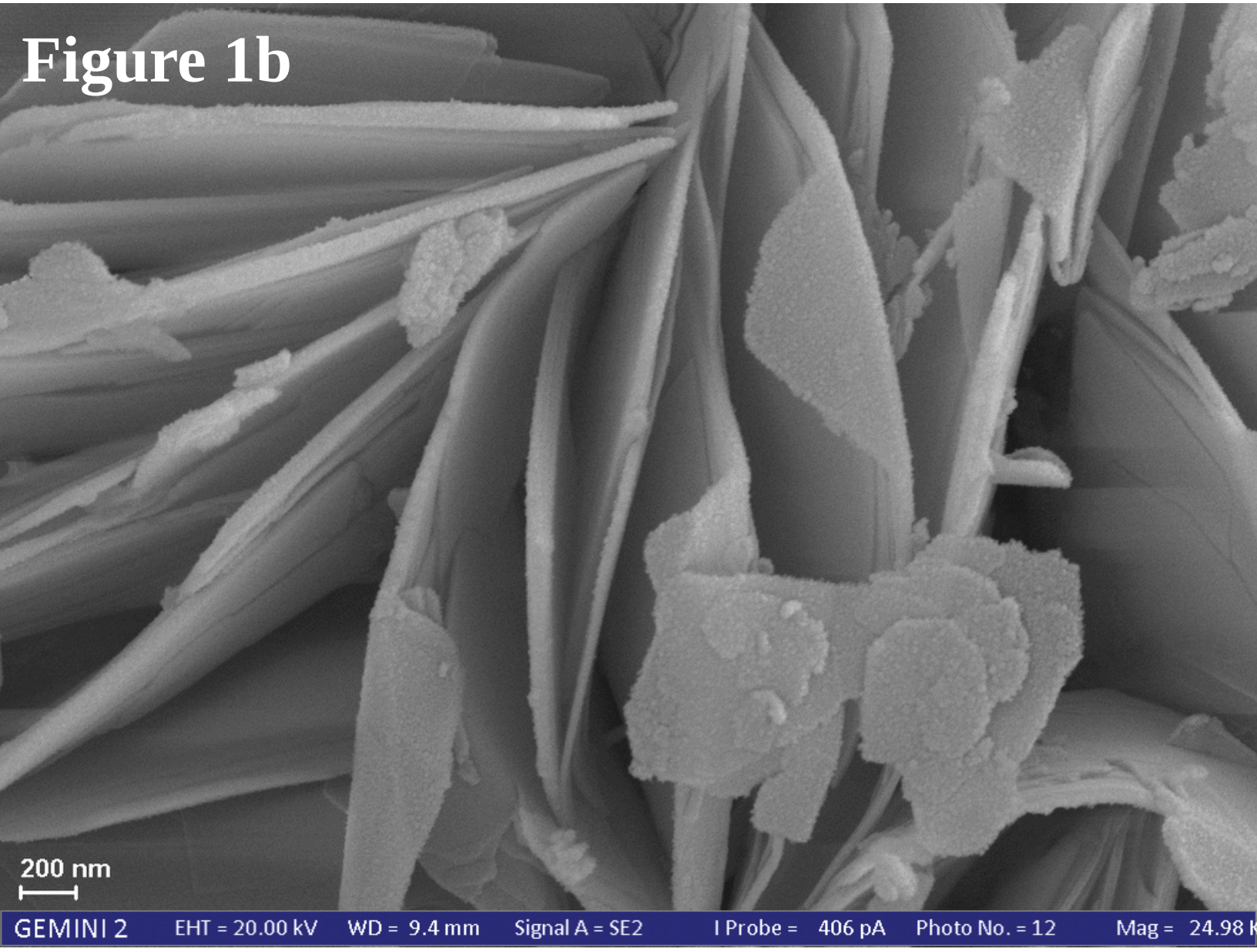
200 nm
GEMINI 2
EHT = 20.00 kV
WD = 9.4 mm
Signal A = SE2
I Probe = 406 pA
Photo No. = 12
Mag = 24.98 K

Figure 1c

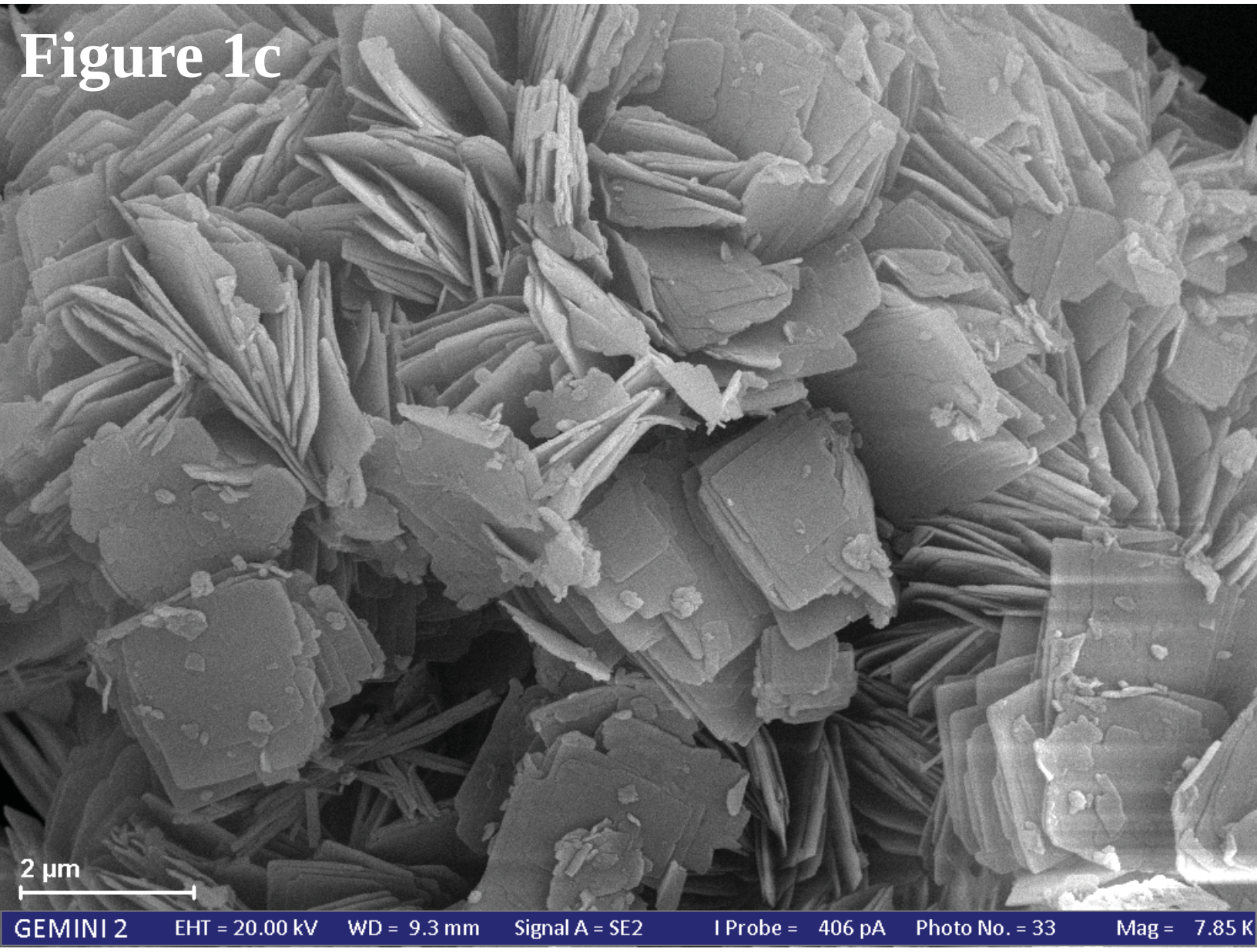
2 µm
GEMINI 2 EHT = 20.00 kV WD = 9.3 mm Signal A = SE2 I Probe = 406 pA Photo No. = 33 Mag = 7.85 K

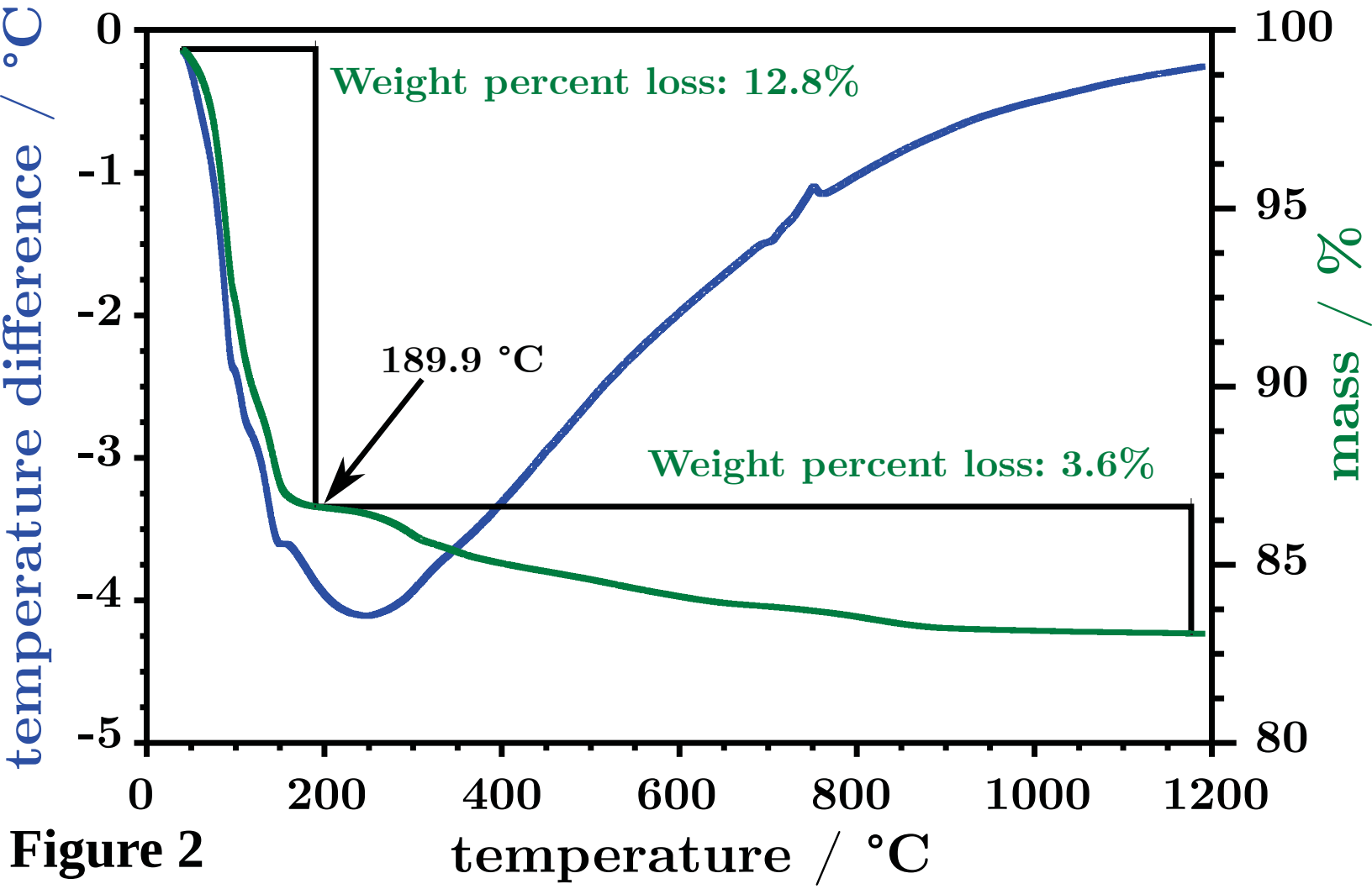
temperature difference / °C
mass / %
temperature / °C
Weight percent loss: 12.8%
189.9 °C
Weight percent loss: 3.6%
0
-1
-2
-3
-4
-5
100
95
90
85
80
0
200
400
600
800
1000
1200

Figure 2

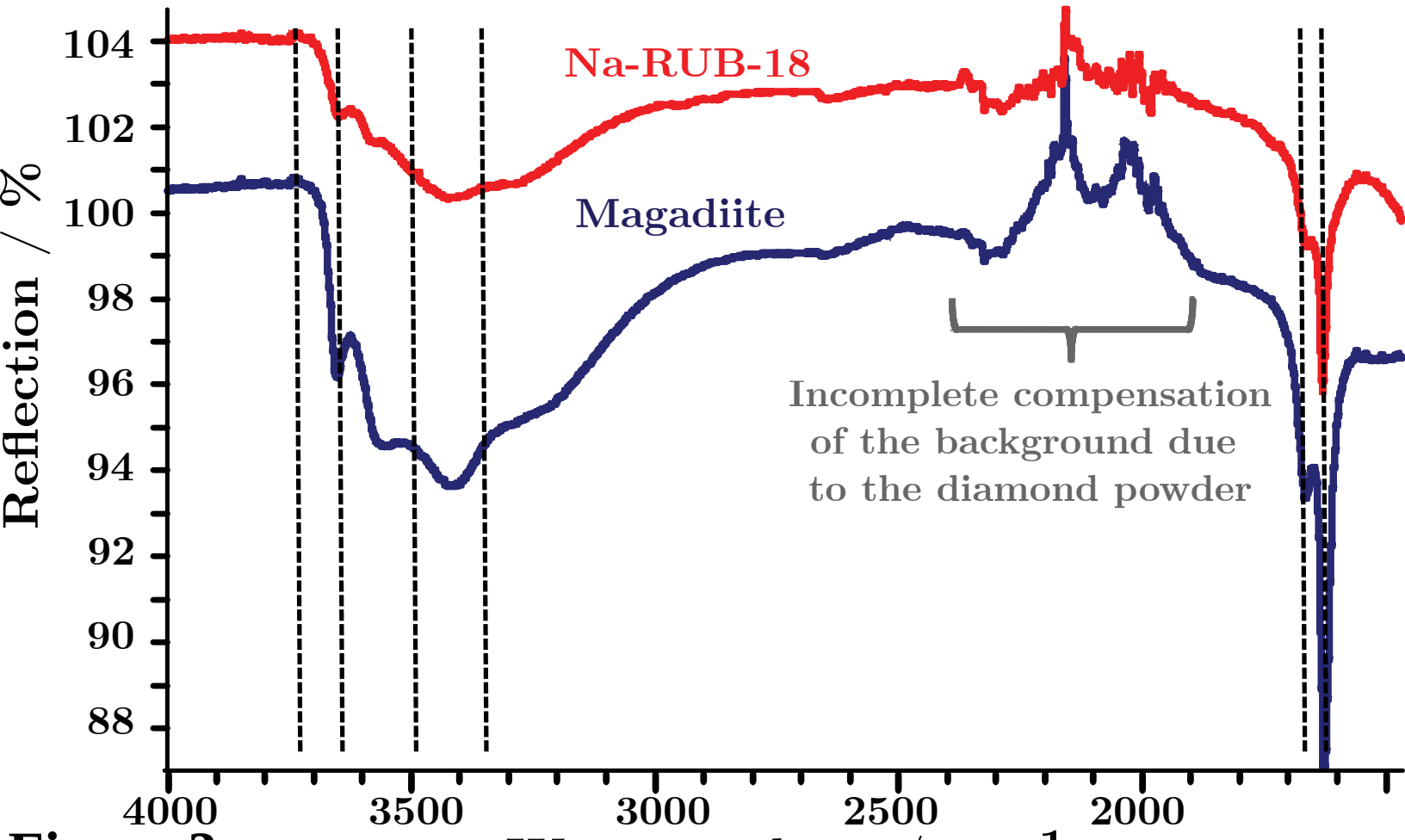
Na-RUB-18
Magadiite
Incomplete compensation
of the background due
to the diamond powder
Reflection / %
104
102
100
98
96
94
92
90
88
4000
3500
3000
2500
2000
Wave numbers / cm-1

Figure 3

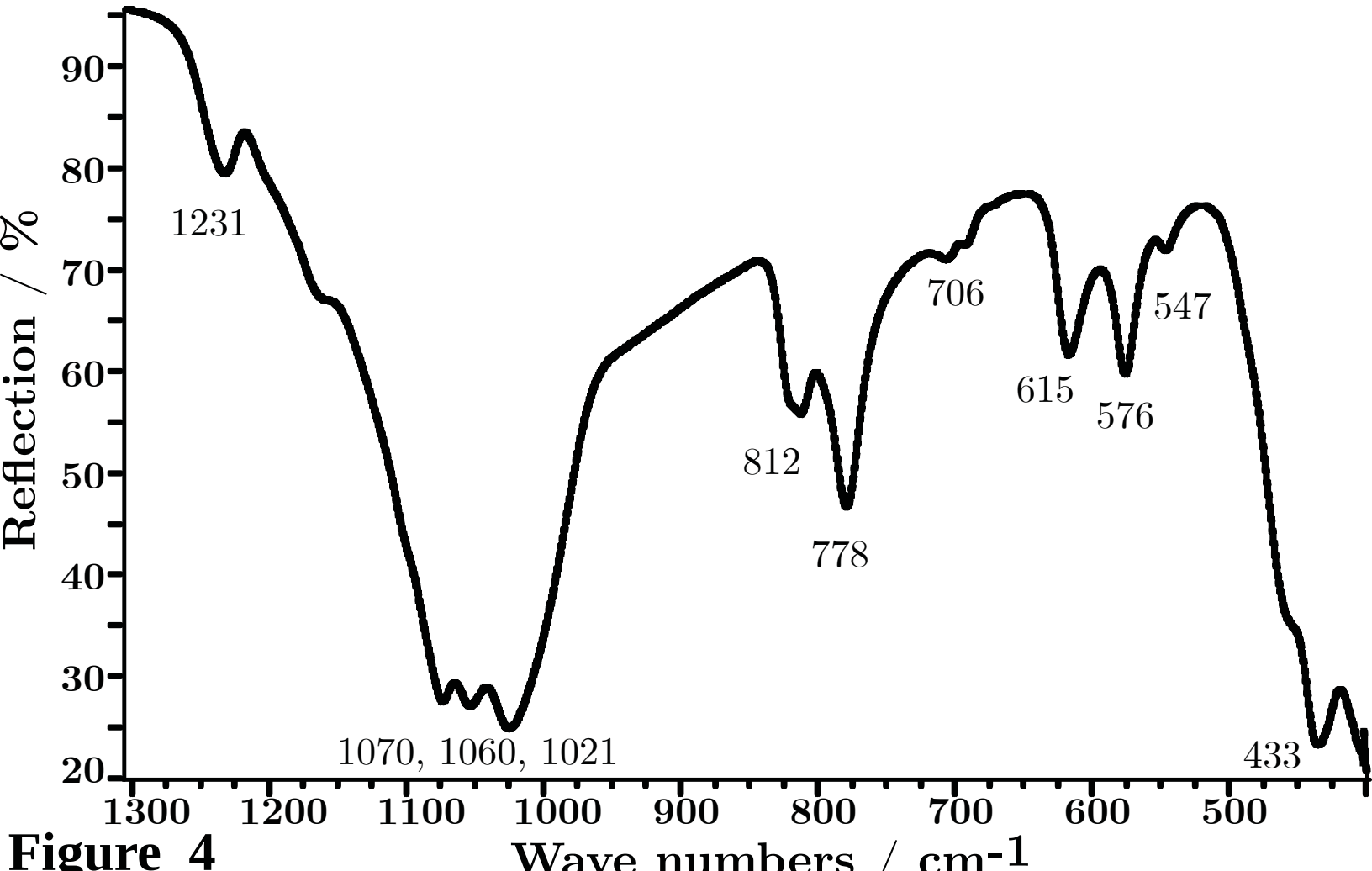
Reflection / %
90
80
70
60
50
40
30
20
1231
1070, 1060, 1021
812
778
706
615
576
547
433
1300
1200
1100
1000
900
800
700
600
500
Wave numbers / cm-1

Figure 4

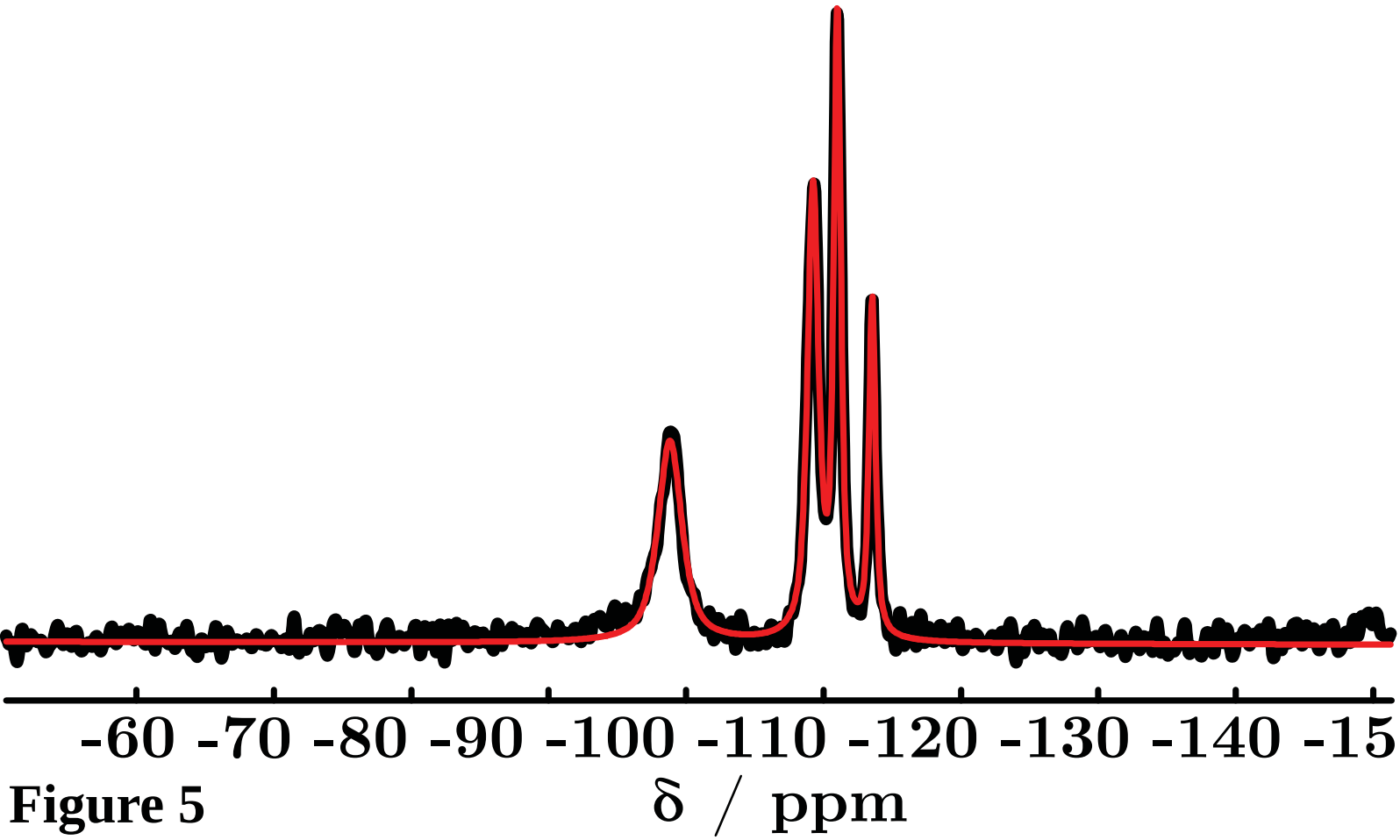

Figure 5

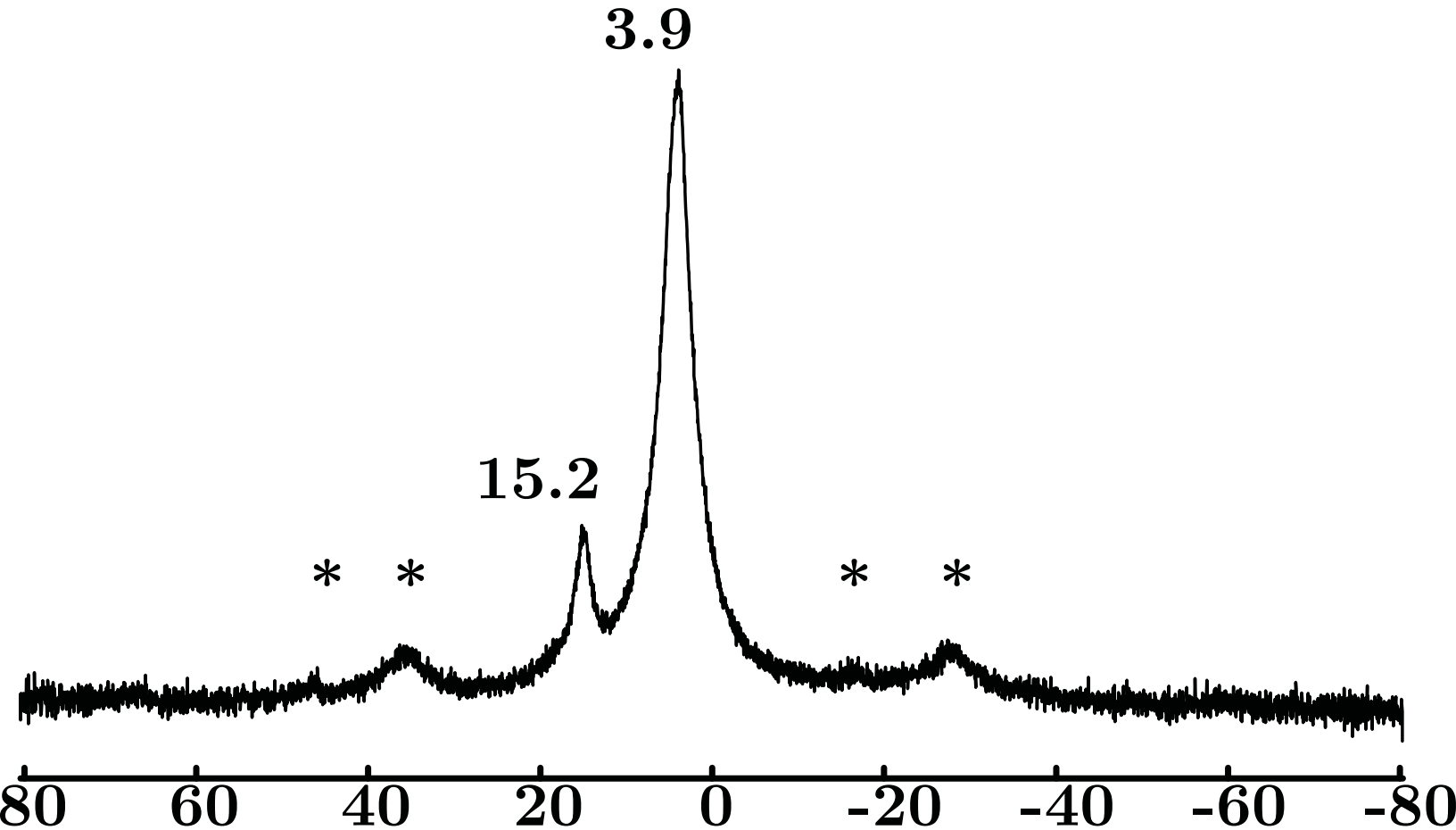

Figure 6

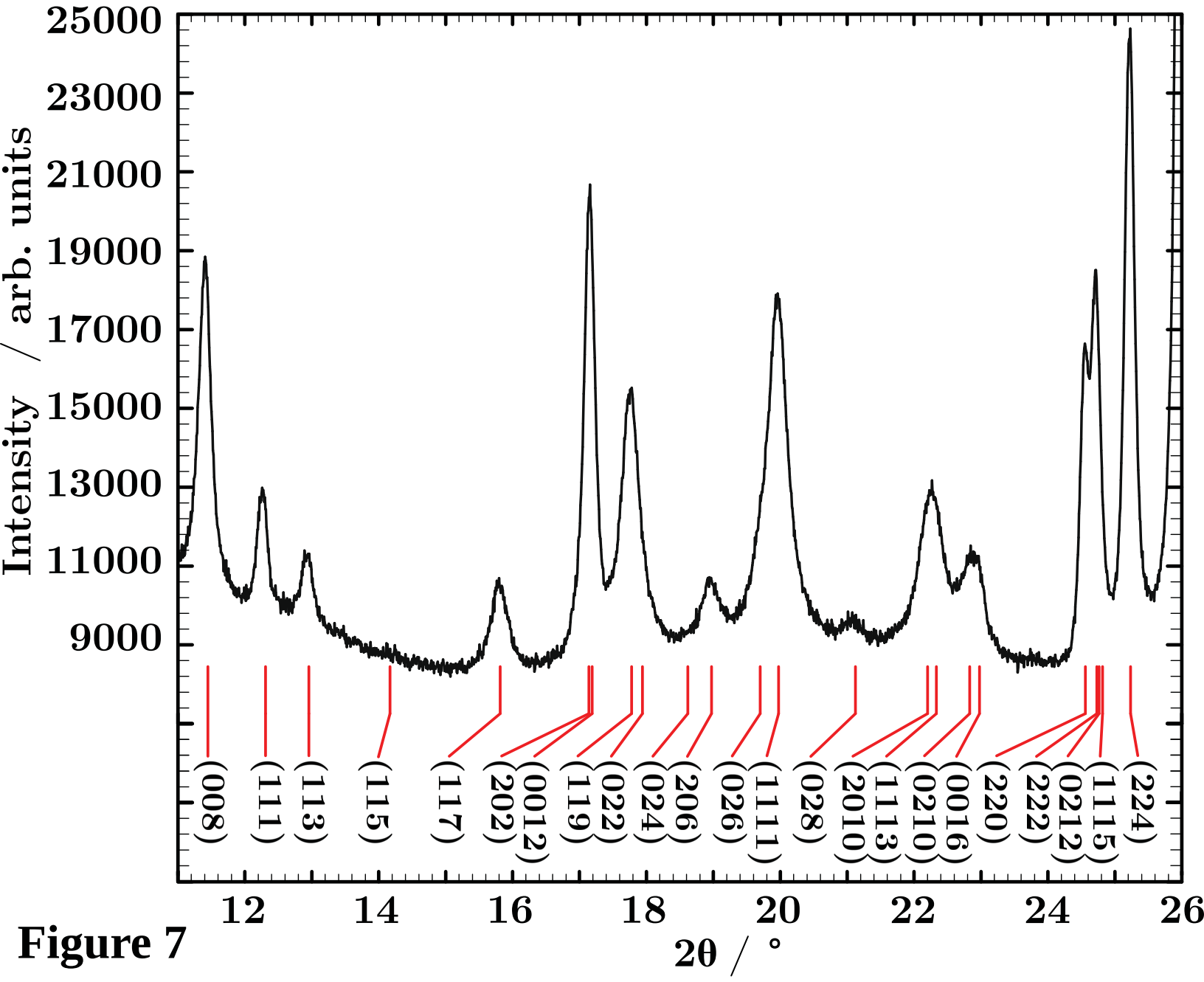
25000
23000
21000
19000
17000
15000
13000
11000
9000
Intensity / arb. units
(008)
(111)
(113)
(115)
(117)
(202)
(0012)
(119)
(022)
(024)
(206)
(026)
(1111)
(028)
(2010)
(1113)
(0210)
(0016)
(220)
(222)
(0212)
(1115)
(224)
12
14
16
18
20
22
24
26
2θ / °

Figure 7

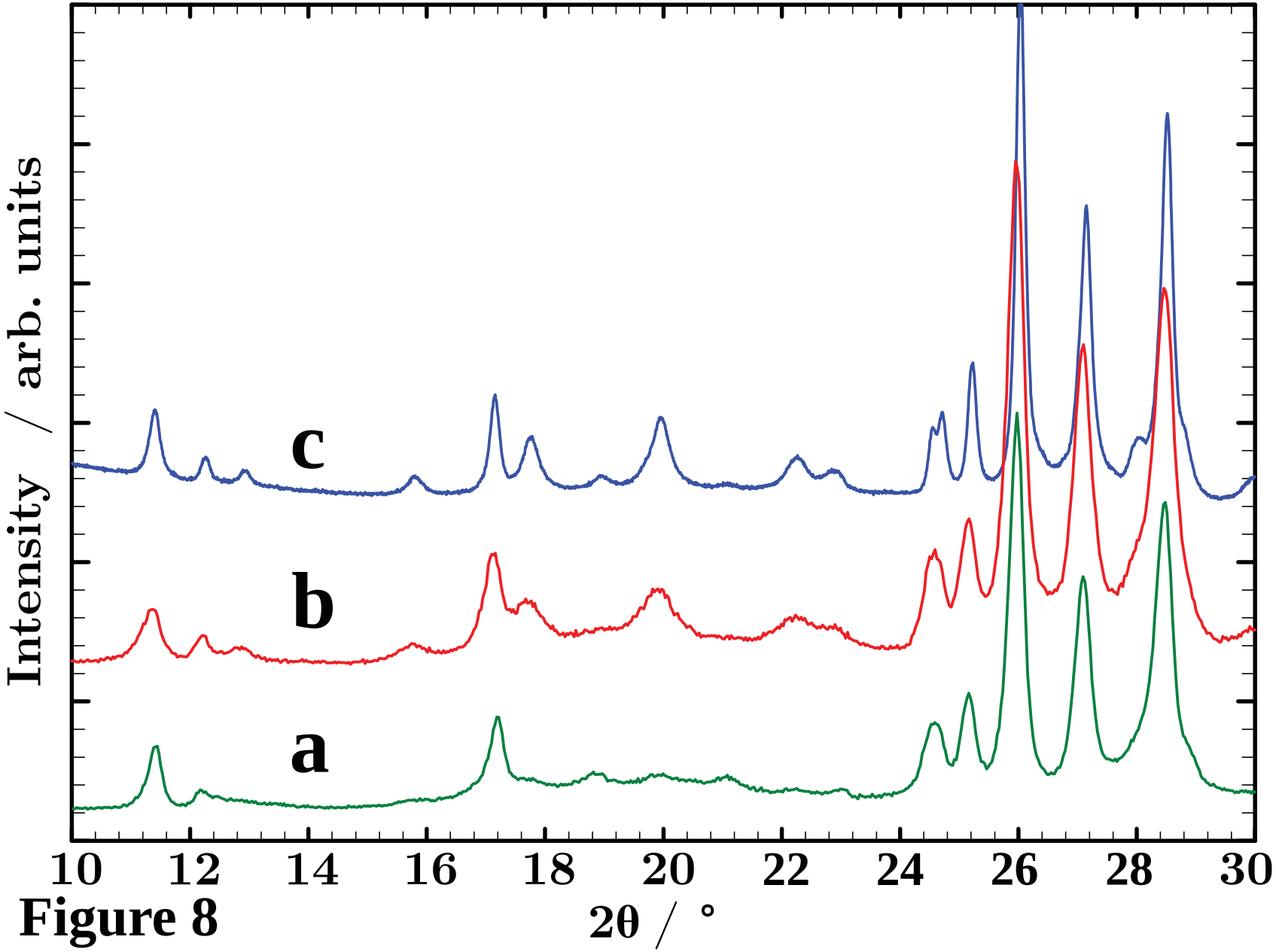

Figure 8

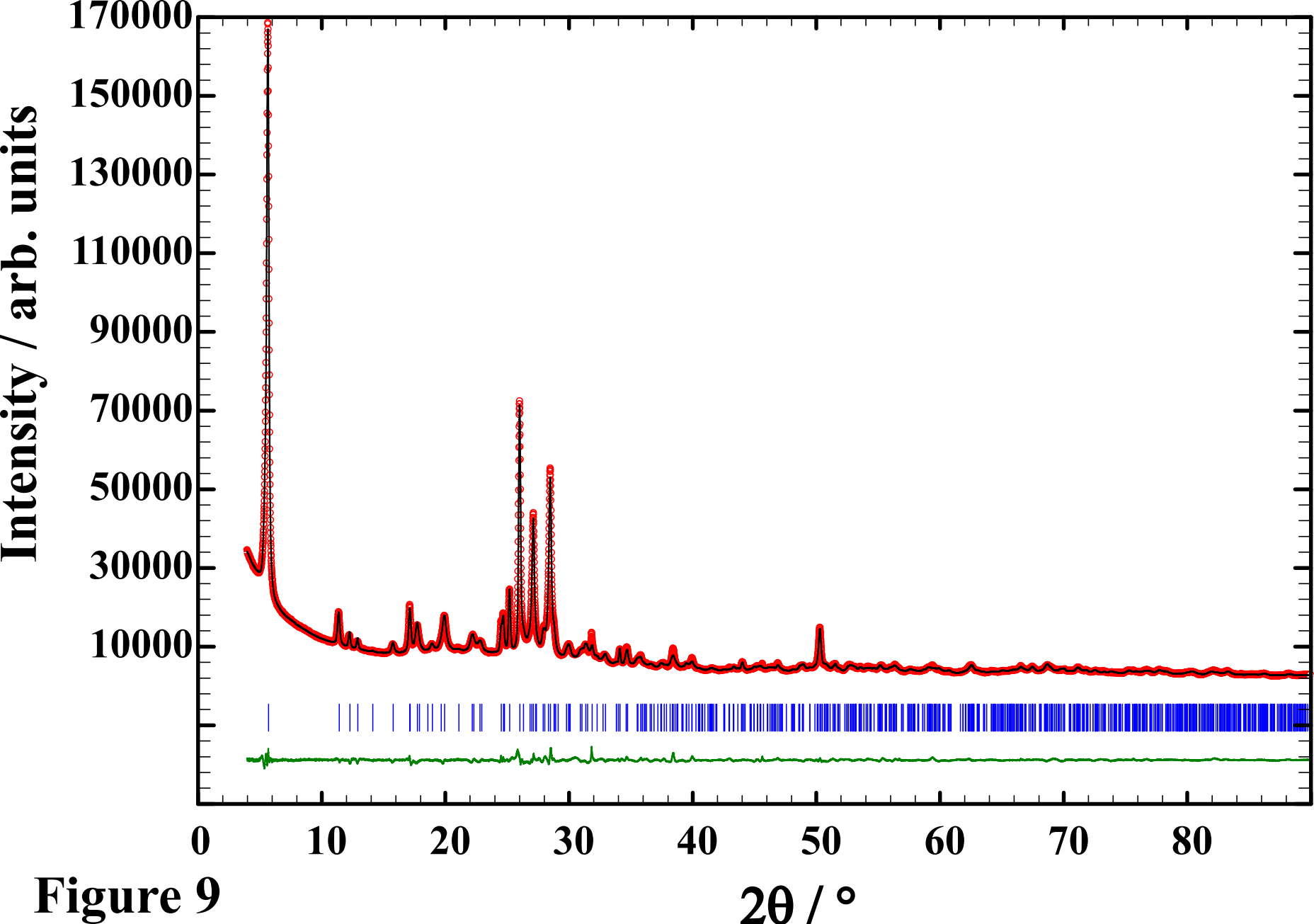
Intensity / arb. units
170000
150000
130000
110000
90000
70000
50000
30000
10000
0
10
20
30
40
50
60
70
80
2θ / °

Figure 9

B

A'

B'

A

B

c_0 = 61.96 Å

c_0 = 45.02 Å

c

a

b

Figure 10

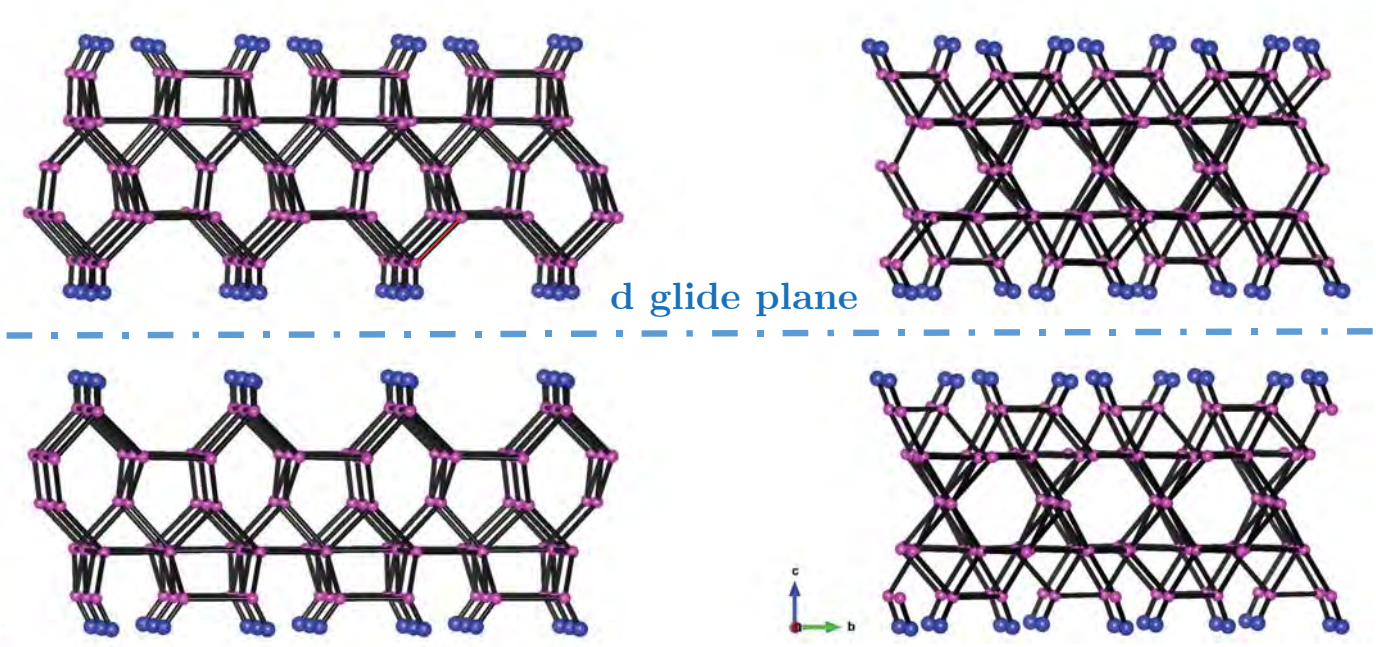

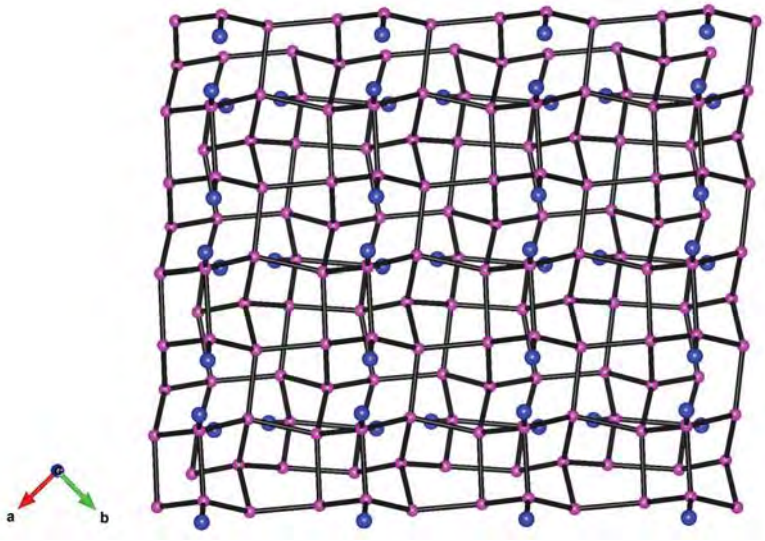

Figure 11

Figure 12

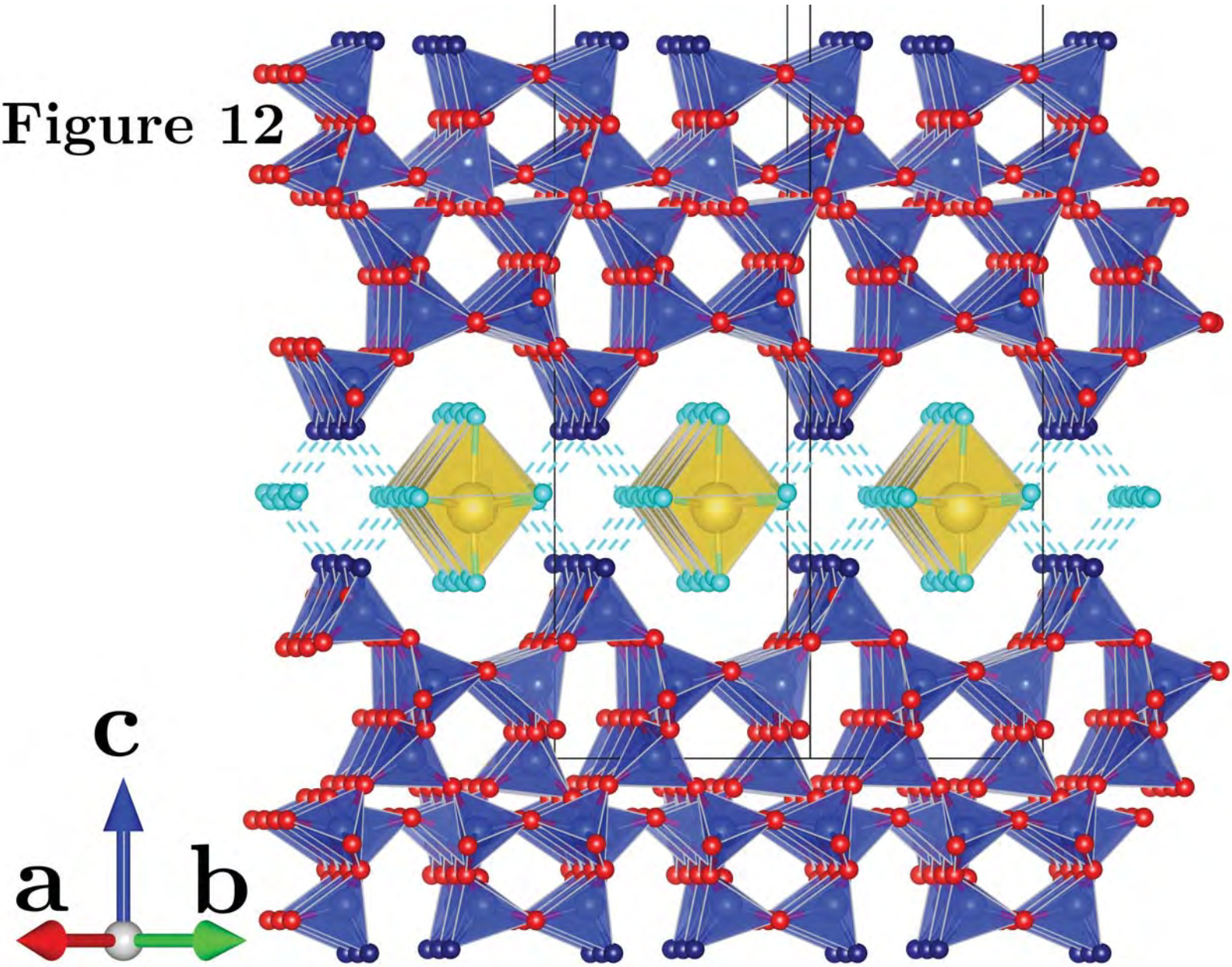

Figure 13

a
Magadiite

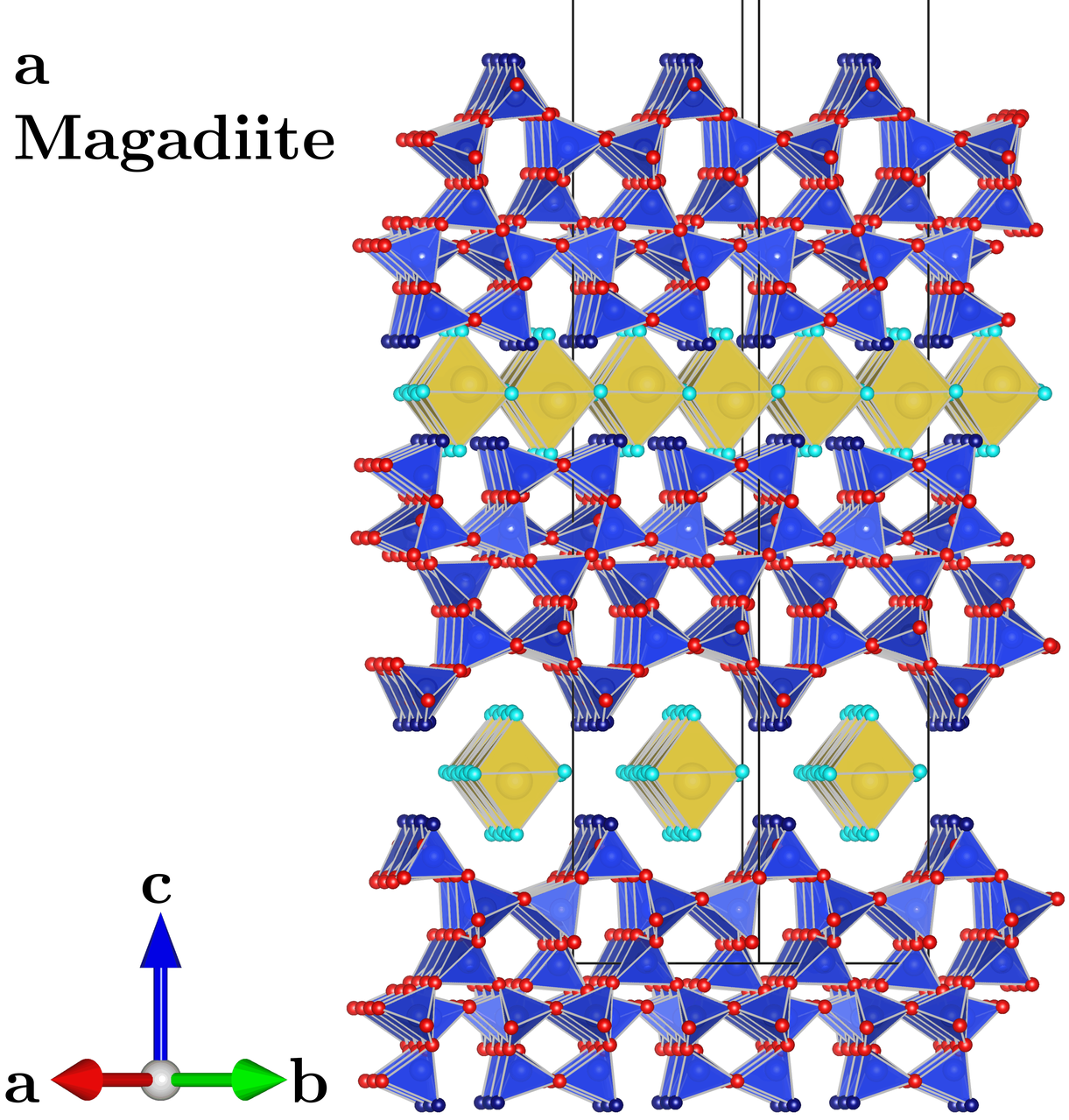

b
RUB-18

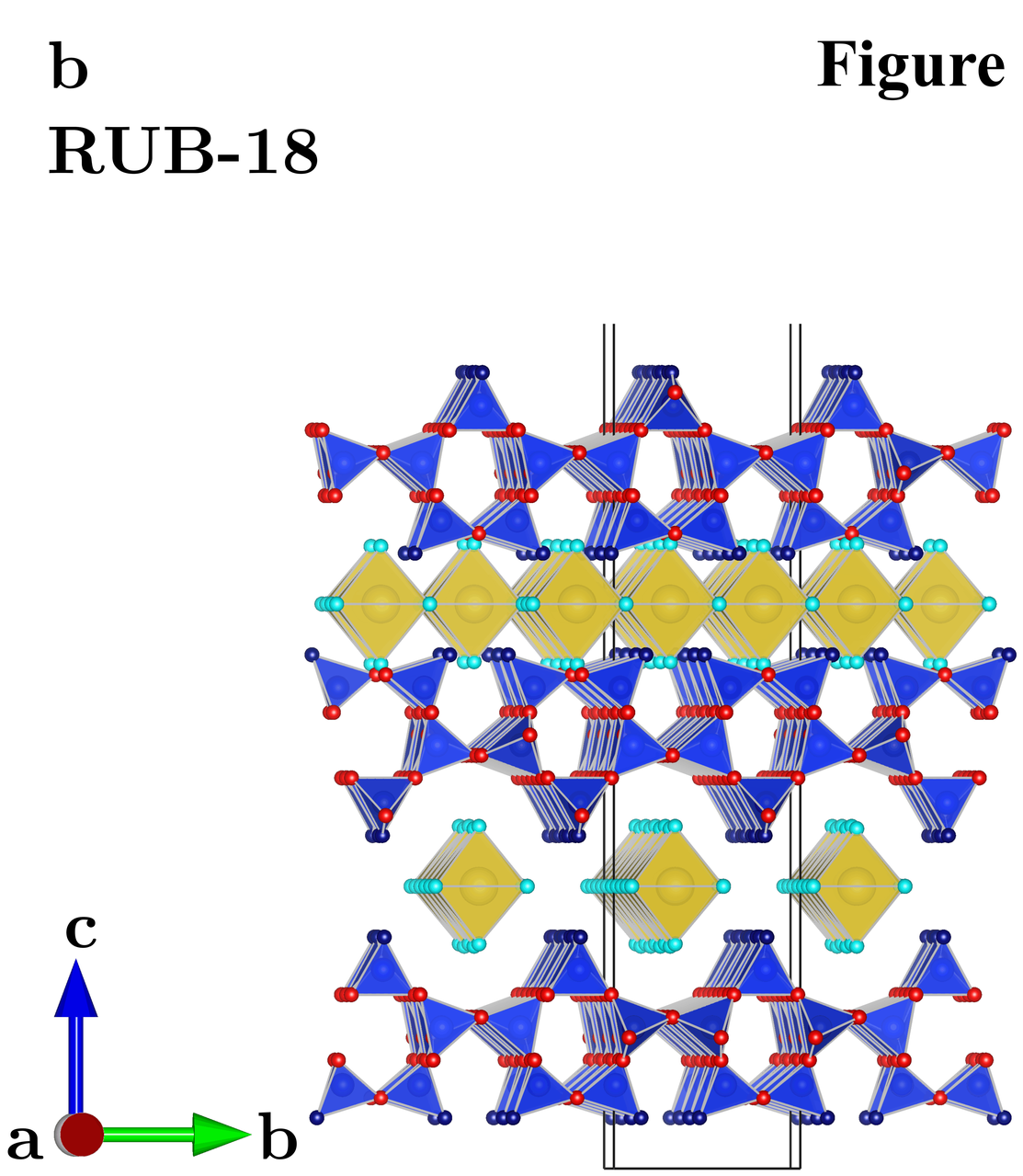

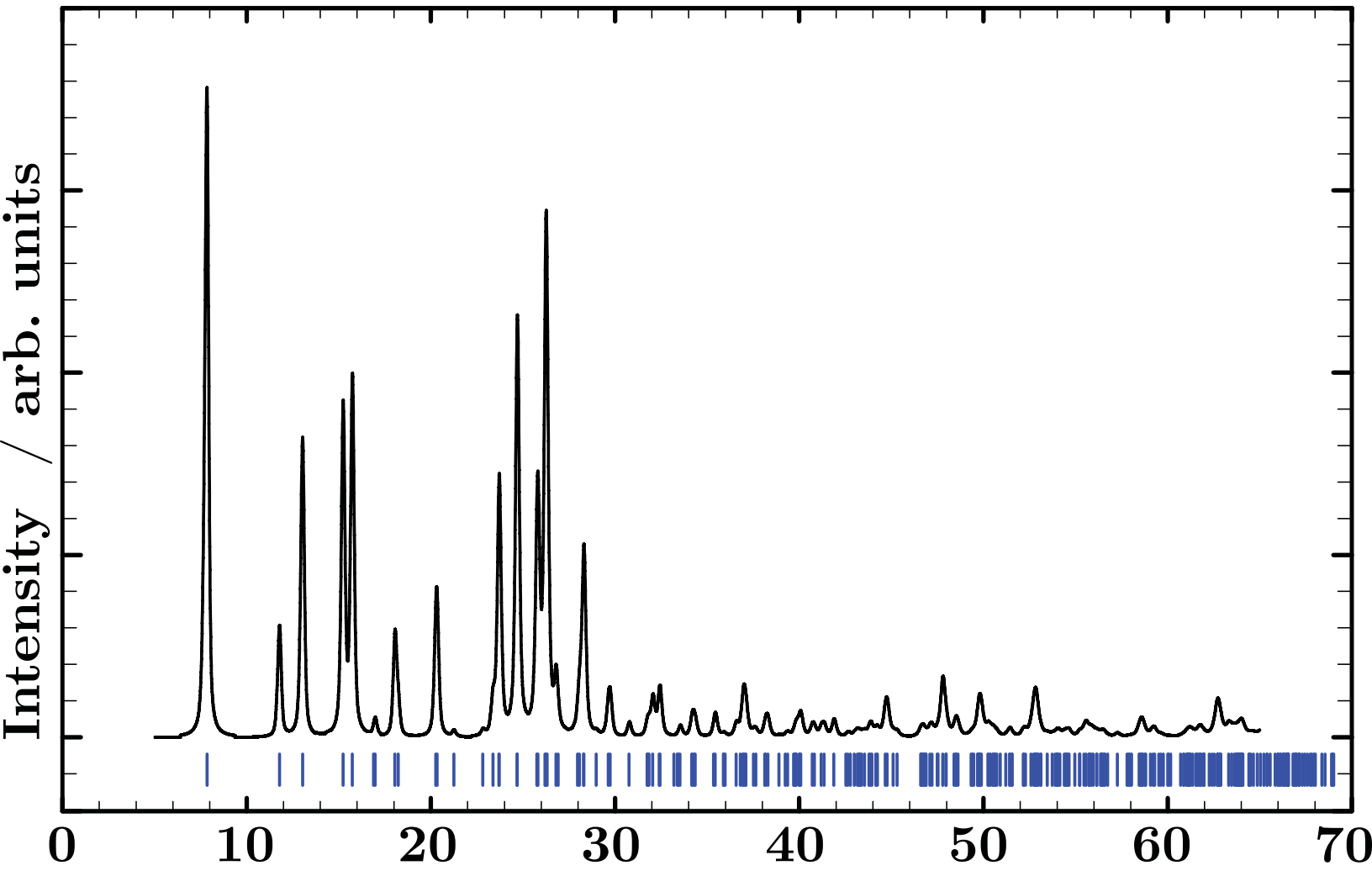

Figure 14